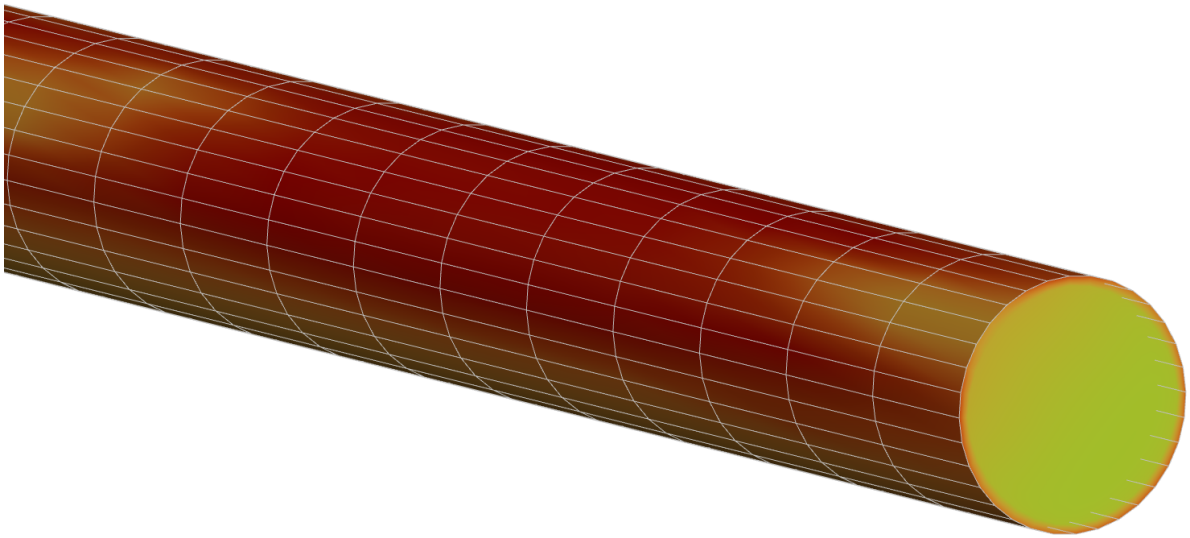

Modelling multiphase heat and mass transfer using a tuned single phase fluid approximation

MMSX30 - Master thesis in Mechanics and maritime sciences

SURAJ SHANKAR

DEPARTMENT OF MECHANICS AND MARITIME SCIENCES

CHALMERS UNIVERSITY OF TECHNOLOGY
Gothenburg, Sweden 2024
www.chalmers.se

Master's thesis 2024

Modelling multiphase heat and mass transfer using a tuned single phase fluid approximation

SURAJ SHANKAR

CHALMERS
UNIVERSITY OF TECHNOLOGY

Department of Mechanics and Maritime Sciences
Division of Fluid Dynamics
Chalmers University of Technology
Gothenburg, Sweden 2024

Modelling multiphase heat and mass transfer using a tuned single phase fluid approximation

SURAJ SHANKAR

Supervisor: Jonas Bredberg and Jonathan Bergh, GKN Aerospace Sweden AB
Examiner: Valery Chernoray, Department of Mechanics and Maritime Sciences

Master's Thesis 2024
Department of Mechanics and Maritime Sciences
Division of Fluid Dynamics
Chalmers University of Technology
SE-412 96 Gothenburg
Telephone +46 31 772 1000

Cover: Vapor quality contour

Typeset in LaTeX
Printed by Chalmers Reproservice
Gothenburg, Sweden 2024

Modelling multiphase heat and mass transfer using a tuned single phase fluid approximation

SURAJ SHANKAR
Department of Mechanics and Maritime Sciences
Chalmers University of Technology

Abstract

Modern aircraft engines are becoming more and more dependent on advanced heat exchanger technology to increase their efficiency and decrease their fuel consumption. This is best demonstrated by the SWITCH WET engine, which recovers waste heat from the exhaust to greatly improve the specific fuel consumption and thermal efficiency of the core engine cycle. The goal of this project is to create computational techniques for modelling the mass and heat transfer mechanisms found in heat exchangers. The important objectives of the thesis were to review the existing pressure drop and heat transfer correlations between water boiling and the creation of a precise tuned model that uses single-phase simulations to mimic water vaporization in a heated tube and validate the model with experimental data. This study provided insight into the tuned material model that was developed as well as how the tuned model affected the two-phase boiling simulation. It was discovered that the model had some errors in its wall temperature prediction. Consequently, the near wall effects of the model were thoroughly investigated, and the influence of thermal conductivity was identified as the source of the issue. On the other hand, the bulk quantities of the flow were accurately predicted by the model. These results contribute to the understanding and validation of the CFD simulations using the tuned model while also highlighting areas where further improvements are necessary. The study further revealed that the prediction of pressure drop along the domain was not trustworthy as the pressure drop was inclined towards a single phase pressure drop of the liquid phase. The error was mainly due to the lower velocity increase with respect to the density change while boiling. The imbalance between the density and velocity would be attributed to the lack of turbulent mixing between the phases which may be a reason for the inaccurate predictions of wall temperature.

Keywords: Heat transfer; modelling; boiling; CFD; multiphase

Acknowledgements

First and foremost, I extend my heartfelt gratitude to my thesis supervisors, Jonas Bredberg and Jonathan Bergh, at GKN Aerospace Engine Systems Sweden, for their unwavering support and guidance throughout this journey. Without their invaluable mentorship, this thesis would not have been accomplished. They have been available to assist me at all times, and the knowledge and experience I gained during the six months of working with him are truly immeasurable. Their role as both a supervisor and mentor has been instrumental in my growth.

Chalmers University has provided excellent support, and I am particularly grateful to Prof. Valery Chernoray from the Fluid Mechanics Department for taking the time to be the examiner for this project.

I would also like to thank my friends for their unwavering support and for always being there to lend a helping hand or provide a much-needed distraction. A special thanks to Alexander Blom Larsen for working with me harmoniously throughout the thesis and for the interesting discussions.

My heartfelt thanks go out to my family for their immense support and encouragement throughout this journey. And lastly, I would like to acknowledge myself for believing in my abilities and staying strong through all the challenges faced.

Suraj Shankar, Gothenburg, June 2024

List of Acronyms

Below is the list of acronyms that have been used throughout this thesis listed in alphabetical order:

API	Application programming Interface
BC	Boiling Crisis
CFD	Computational Fluid Dynamics
CHF	Critical Heat Flux
ONB	Onset of Nucleate Boiling
HTC	Heat Transfer Coefficient
UDF	User Defined Function
UDM	User Defined Memory

Nomenclature

Below is the nomenclature of variables and subscripts that have been used throughout this thesis.

Parameters

h	Heat transfer coefficient
T	Temperature
q	Total surface heat flux
u	Flow velocity
L	Characteristic length
k	Thermal conductivity
ρ	Density
μ	Dynamic viscosity
k	Turbulent kinetic energy
ϵ	Turbulent dissipation rate
ω	Specific dissipation rate
c_p	Specific heat
Re	Reynolds number
Pr	Prandtl number
Nu	Nusselt number
h	Enthalpy
h_{lv}	Heat of Vaporization
G	Mass flux
$\dot{m}$	Mass flow rate
d, D	Diameter

Subscripts

cr	Critical
$fric$	Friction
L,l	Liquid
in	Inlet
out	Outlet
sat	Saturation
sub	Subcooled
v	Vapor
w	Wall value
eff	Effective quantity

Contents

List of Figures

List of Tables

1
Introduction

1.1 Background

The goal of the Sustainable Water-Injecting Turbofan Comprising Hybrid-Electrics (SWITCH) project is to create a new propulsion concept based on the innovative and complementary technologies of hybrid-electric propulsion and Water-Enhanced Turbofan (WET) which is illustrated in Figure 1.1. WET has the potential to greatly increase efficiency and lower overall emissions for aviation propulsion systems in the future, regardless of whether they run on hydrogen, SAF, or ordinary kerosene which can be seen in [1][2]. An integral part of the engine is the heat exchanger.

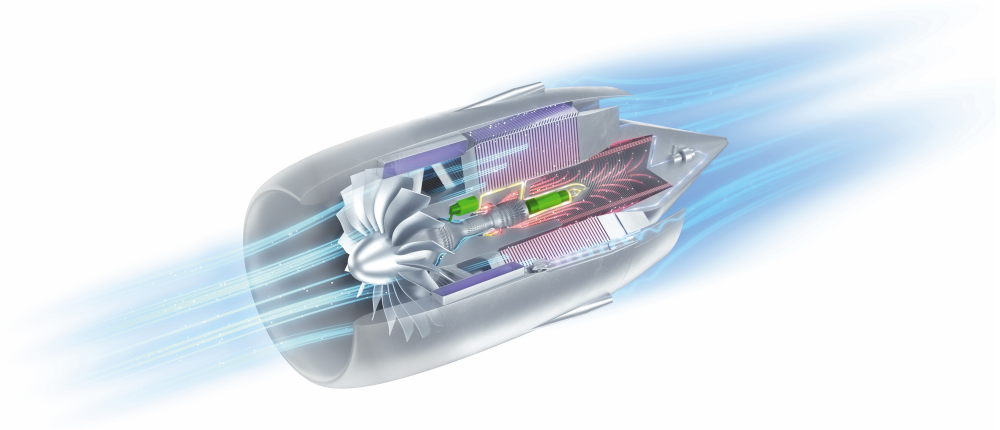

Figure 1.1: The SWITCH WET concept aero engine. Reproduced from [1]

Recovering the exhaust energy that would otherwise be lost improves engine efficiency and reduces fuel and CO2 emissions. A vaporizer first generates hot steam and in the process, the exhaust gas cools down. As the gases cools down in the condenser, the water within starts to condense. A water separator separates the liquid water from the exhaust gas while the condensation heat is given to the bypass flow. In the process, condensation nuclei are also removed from the exhaust gas, minimizing the creation of contrails. After that, a pump raises the water's pressure before delivering it to the steam generator. In a steam turbine, the steam expands before entering the combustor. The low-pressure shaft receives the power input. Not only does injecting hot steam into the combustor improve engine efficiency, but it also lowers emissions of nitrogen oxide (NOx).

1.2 Aim

The aim of the thesis is to review the literature regarding correlations for multiphase heat transfer and pressure drop for flows through a horizontal pipe in a heat exchanger and then develop or determine a representative set of tuned material properties and to produce a design code for two phase flow in heat exchangers to emulate experimental data taken from a research paper.

1.3 Difficulties and Proposition

Computational modelling of multiphase systems which includes mass and heat heat transfer is often found difficult. This is because one or more equations for the turbulence properties, energy, mass, and energy conservation equations of each phase may be included in a multiphase system. Furthermore, complex sub models may be used to represent these processes, depending on the type of physical mechanism (evaporation, boiling, or condensation) through which the mass exchange occurs. All in all, this leads to a situation where these simulations inevitably become complex and numerically instable.
To overcome these challenges, a simpler, less computationally demanding method that uses a single phase material with tuned properties may be used to simulate the transition of the flow medium between phases. A single phase tuned model is likely to be much faster, easier to set up, and easier to solve due to the elimination of the secondary phase and the requirement to transfer mass and energy between different phases, while still producing results that are accurate enough to model many multiphase systems.

1.4 Methodology

The important milestones in the thesis include the review of existent literature for correlations involving heat transfer and pressure drop for water boiling in the heat exchanger tubes. With the knowledge gained from the literature, a suitable tuned model has to be developed and compared with an experimental literature available. With the developed tuned fluid, a single phase simulation is performed in ANSYS Fluent which mimics the vaporization process of water in a heated tube. Ultimately, the results from the simulation are compared with the experimental data from a research paper and in turn build an engineering tool for multiphase flow in heat exchanger tubes.

2

Theory

2.1 Theory

2.1.1 Fluid Mechanics

The discipline that studies how fluids behave when at rest (fluid statics) or when they are moving (fluid dynamics) as well as how they interact with solids or other fluids at boundaries is known as fluid mechanics.

2.1.1.1 Fluid Flow Regime

Laminar and turbulent flow behaviors are the two basic regimes in fluid flows shown in Figure 2.1. The flow behaves smoothly and predictably in the laminar regime. This indicates that there is little to no mixing between adjacent levels as the fluid particles travel smoothly in parallel layers. In this case, the flow represents consistent and dependable behavior. Conversely, the turbulent regime is distinguished by erratic and unpredictable variations in the flow. Due to the swirling eddies and random velocity fluctuations form, turbulent flows are highly mixed and unpredictable. Transition flow describes the modification of flow behavior that takes place when a flow moves from a laminar to a turbulent regime which is a highly disordered fluid motion which typically occurs at high velocities and is characterized by velocity fluctuations.

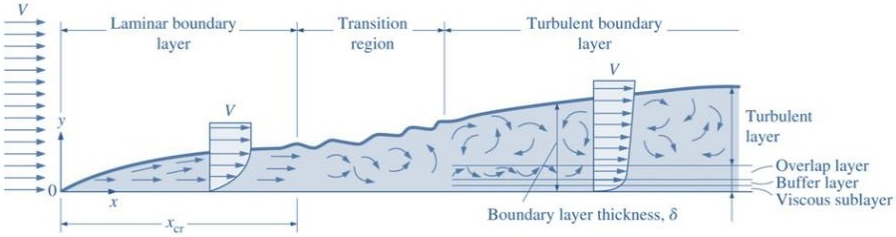

Figure 2.1: Boundary layer fluid flow regimes [3]

2.2 Heat Transfer

The process of exchanging thermal energy between various areas of a physical system or between systems is known as heat transfer. Heat flows from regions of higher

temperature to regions of lower temperature due to thermal gradients. The main modes of heat transfer are conduction, convection, and radiation.

2.2.1 Heat Conduction

Heat conduction is the transfer of thermal energy through a material or between materials that are in direct contact, driven by a temperature difference.
The rate at which heat is transferred by conduction, q_k, is proportional to the product of the temperature gradient, $\frac{dT}{dx}$, and the cross-sectional area A through which the heat transfer occurs.

$$q_k = -kA\frac{dT}{dx} \tag{2.1}$$

Where k is the thermal conductivity of the material.

2.2.2 Convection

Convection is the heat transfer through fluid movements. Convection can occur either naturally or be forced. If a fluid is pushed to flow over the surface by an outside force, like the wind, a pump, or a fan, it is referred to as forced convection. Conversely, when buoyancy forces resulting from temperature variations in the fluid generate density differences that drive fluid motion, convection is referred to as natural (or free) convection.
Irrespective of the mechanism, the rate of heat transfer by convection is given by,

$$q_c = h_c A \Delta T \tag{2.2}$$

Where:

- q_c is the rate of heat transfer by convection
- A is the area of heat transfer
- ΔT is the difference between the surface and the fluid temperature
- h_c is the convection heat transfer coefficient

2.2.3 Radiation

Radiation is the transfer of heat through electromagnetic waves, in the form of infrared radiation. In contrast to conduction and convection, radiation can travel in a vacuum and doesn't need a medium to do so. Any object that has a temperature higher than zero produces heat radiation. The radiation heat loss can be expressed as,

$$q_r = \varepsilon \sigma T^4 A \tag{2.3}$$

Where:

- q_r is the rate of heat transfer by radiation
- ε is the emissivity coefficient of the object
- A is the area of the emitting body
- T is the temperature

- σ is the Stefan-Boltzmann constant, which is $5.6703 \times 10^{-8}\,\mathrm{W/m^2K^4}$

2.2.4 Overall Heat Transfer

The overall heat transfer is expressed as

$$q = U_{\text{overall}} A \Delta T_{\text{total}} \tag{2.4}$$

Where:

- U_{overall} is the overall heat transfer coefficient

More specifically, the product of the overall coefficient and the area is the inverse of the sum of the thermal resistances, i.e.,

$$\frac{1}{U_{\text{overall}} A} = R_{\text{total}} \tag{2.5}$$

Where R_{total} can be defined as the sum of resistances.

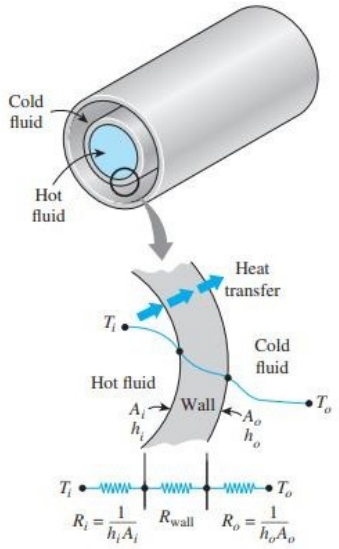

Figure 2.2: Thermal resistance network from [4]

$$R_{\text{total}} = \frac{1}{h_i A_i} + \frac{\ln\left(\frac{D_o}{D_i}\right)}{2\pi k L} + \frac{1}{h_o A_o} \tag{2.6}$$

Equation (6) gives the total resistance for the thermal resistance network associated with heat transfer in a double pipe heat exchanger which is shown in Figure 2.2.

2.3 Mass Transfer

Mass transfer is a phenomenon characterized by the movement of one or more species within a medium or across interfaces, driven by concentration gradients. This process occurs in a range of physical and reactive systems and includes diffusive, convective, and reactive transport mechanisms.

There is no heat transfer involved in the majority of mass transfer processes that exist in practice since they happen isothermally. However, in some technical applications, as shown in Figure 2.3, a liquid will vaporize and then diffuse into the surrounding atmosphere. Such procedures involve simultaneous mass and heat transfer when the latent heat of vaporization (h_{fg}) is added into the liquid and evaporates it. In general, heat transfer must be a part of any mass transfer problem involving phase change (evaporation, sublimation, condensation, melting, etc.), and the solution of such problems must be examined by taking simultaneous heat and mass transfer into account.

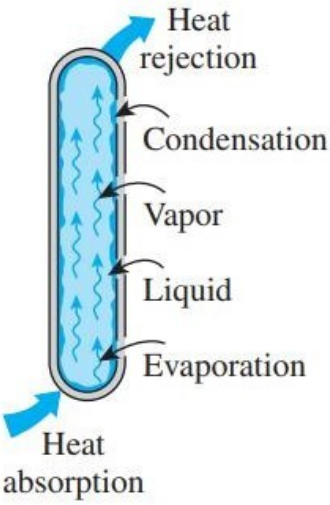

Figure 2.3: Simultaneous mass and heat transfer [4]

2.4 Important Dimensionless Numbers

2.4.1 Reynolds Number, Re

Reynolds number is the ratio between the inertial forces and the viscous forces. Reynolds number can be expressed as:

$$\mathrm{Re} = \frac{\rho u L}{\mu} \tag{2.7}$$

Where:

- ρ is the density of the fluid, kg/m^3
- u is the flow velocity, m/s
- L is the characteristic length, m
- μ is the dynamic viscosity, Pa.s

Reynolds number is very crucial in determining the nature of the flow, i.e., if the flow is laminar or turbulent. For flow within a tube, the flow regime can be classified based on the Reynolds number (Re). When Re exceeds 3500, the flow is characterized as turbulent. Conversely, when Re is below the critical value of 2300, the flow is considered laminar. Flow conditions between these two Reynolds numbers fall within the transitional regime.

2.4.2 Boiling Number, Bo

Boiling number, Bo, is used to analyze two-phase flows for cases like boiling heat transfer. The mathematical representation of the boiling number is:

$$\mathrm{Bo} = \frac{q}{H_{lg} G_l} \tag{2.8}$$

Where:

- q is the heat flux, W/m^2
- H_{lg} is the latent heat of vaporization, kJ/kg
- G_l is the mass flux of the liquid phase, kg/m^{2}s

Boiling number can also be defined as the ratio between the heat transfer coefficient due to boiling and the heat transfer coefficient due to convection. If the boiling number is greater than 1, then the heat transfer is dominated by boiling and vice versa. The boiling number helps us understand the flow regime as well as the dominance of heat transfer, which helps in designing better systems. In addition, the boiling number is important for safety considerations in systems where phase change occurs.

2.4.3 Prandtl Number, Pr

Prandtl number is a dimensionless quantity that gives the ratio between momentum diffusivity and thermal diffusivity.
The thermal diffusivity is given as:

$$\alpha = \frac{k}{\rho C_p} \tag{2.9}$$

And momentum diffusivity is given as:

$$\nu = \frac{\mu}{\rho} \tag{2.10}$$

Prandtl number is expressed as:

$$\mathrm{Pr} = \frac{C_p \mu}{k} \tag{2.11}$$

Where:

- C_p is the specific heat, J/kg K
- k is the thermal conductivity, W/m K
- μ is the dynamic viscosity, Pa s

In the design and study of heat exchangers and other thermal systems where the interaction between fluid motion and heat transfer is important, an understanding of the Prandtl number is essential. For example, gases typically have lower Prandtl numbers than liquids, indicating that thermal diffusivity is dominant in the flow of gases.

2.4.4 Nusselt Number, Nu

A dimensionless metric used in heat transfer to describe the ratio of convective heat transfer to conductive heat transfer over a boundary layer is the Nusselt number, or Nu for short. The Nusselt number quantifies the effect of convection due to the fluid motion compared to conduction. When Nu is more than unity, the heat transfer is dominated by convection.
The equation for finding the Nusselt number is given as:

$$\mathrm{Nu} = \frac{hL}{k} \tag{2.12}$$

Where:

- h is the convective heat transfer coefficient, W/m^{2}K
- k is the thermal conductivity, W/m K
- L is the characteristic length, m

2.4.5 Schmidt Number, Sc

The Schmidt number of a fluid is a dimensionless number defined as the ratio of momentum diffusivity to mass diffusivity and it is used to characterize fluid flow where both simultaneous mass and momentum diffusion convection processes occur. The Schmidt number is defined as:

$$\mathrm{Sc} = \frac{\nu}{D} \tag{2.13}$$

Where:

- ν is the kinematic viscosity, m^2/s
- D is the mass diffusivity, m^2/s

2.4.6 Vapor Quality, x

In thermodynamics and fluid mechanics, the percentage of a saturated mixture in the vapor phase is referred to as vapor quality. It is especially pertinent to the study of two-phase flow and phase transitions in systems like refrigeration cycles, condensers, and boilers. Vapor quality is defined as the mass percentage of vapor in a liquid-vapor mixture and is represented by the symbol x. It falls between 0 and 1. Vapor quality can be calculated by dividing the mass of the vapor by the mass of the total mixture,

$$x = \frac{m_{\text{vapor}}}{m_{\text{mixture}}} \tag{2.14}$$

An alternative definition for vapor quality, which is valid only for a single component mixture like, for example, water with steam is:

$$x = \frac{h - h_f}{h_{fg}} \tag{2.15}$$

Where:

- h is the enthalpy of the mixture

- h_f is the saturation enthalpy of the liquid
- h_{fg} is the latent heat of vaporization

2.5 Boiling

Boiling is a phase transition phenomena that occurs when the heating wall is kept above the boiling medium's saturation temperature. In the same way as evaporation, boiling is a liquid-to-vapor phase shift process, although the two are not the same. When the vapor pressure at a particular temperature is lower than the saturation pressure of the liquid, evaporation takes place at the liquid–vapor interface. On the other hand, boiling happens at the solid–liquid interface when a liquid comes into contact with a surface that is kept at a temperature that is higher than the saturation point of the liquid.
Boiling can be categorized according to the fluid container's geometry1 or the phase change mechanism. Like single phase forced convection heat transfer, it can also be categorized as merely external or internal boiling.

2.5.1 Classification of boiling

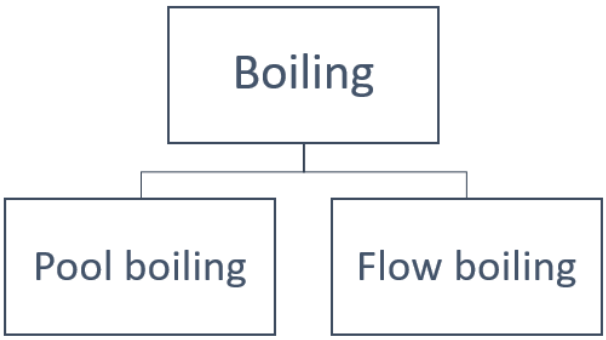

Figure 2.4: Classification based on geometry

The classification of boiling based on the geometry and the flow conditions can be seen in Figure 2.4 which is explained by Cengel [4] and further illustrated in Figure 2.5. The term pool boiling refers to the heat addition to a liquid which is stagnant in a pool. The most common example of pool boiling is the boiling of water in a pot. Often, pool boiling is referred to as 'External boiling'.
On the contrary, 'Internal boiling' is a common term used for flow boiling. Flow boiling or forced convection boiling refers to the boiling that usually occurs while the liquid is forced to flow inside pipes or ducts. In case of flow boiling, there is change not only in the phase from liquid to vapor but also a change in the flow pattern

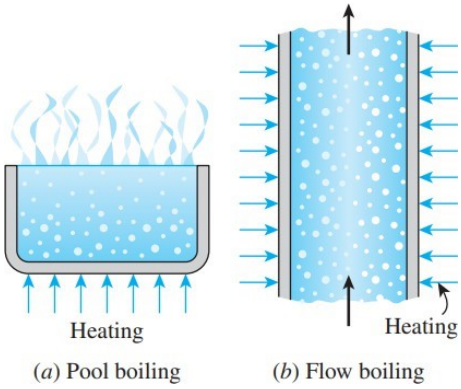

Figure 2.5: Boiling types [4]

2.5.1.1 Pool boiling

The term "pool boiling" describes the boiling process that takes place when a heated surface is in contact with a liquid reservoir. During pool boiling, vapor bubbles are created when the liquid close to the heated surface absorbs heat and reaches its boiling point. Because of buoyancy, these bubbles separate from the liquid's surface and ascend through it. They pass heat into the surrounding liquid as they rise, and eventually they collapse near the surface or in the liquid's bulk. More bubbles continue to form and rise during the procedure, maintaining a continual boiling process. The categorization of pool boiling given by Llic et.al [5] is shown in Figure 2.6.

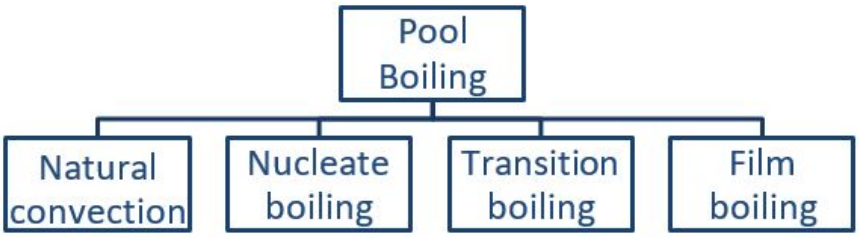

Figure 2.6: Pool boiling

- Heat gets transferred from the heated surface to the liquid through natural convection and conduction before boiling occurs. As the cooler liquid from above moves below to replace the warmer, less dense liquid in contact with the heated surface, it rises upward.
- Nucleate boiling is a form of boiling that occurs when the heat flow is below the critical heat flux but the surface temperature is higher than the saturated fluid temperature. During nucleate boiling, the vapor bubbles that are formed on the surface detach, and this is known as the Onset of Nucleate Boiling (ONB), which is shown in Figure 2.7. It is the beginning of the boiling process and is most often known for its enormous potential for transferring heat when compared with single-phase flow.

- As the upper limit of the nucleate boiling leg is reached, Boiling Crisis (BC) occurs and the boiling system can follow two paths. One possible outcome would be if there is any further increase in the wall superheat, the heat transfer rate will decrease and it will lead to the transition boiling regime. The contact state on the heating surface, which transitions from a partial liquid film to a complete vapor layer, is what causes the transition boiling leg's peculiar negative slope. Leidenfrost point is the place where the leg of film boiling and the transition boiling leg meet.
- Another possible outcome, which is common in power-controlled systems, is if there is any further increase of wall heat flux, it leads to a sudden vapor layer over the surface and this will lead to a direct jump to the regime of film boiling. This transition from a nucleate to a film boiling regime is followed by a significant rise in wall superheat and may cause damage to the heating surface, also referred to as burnout.

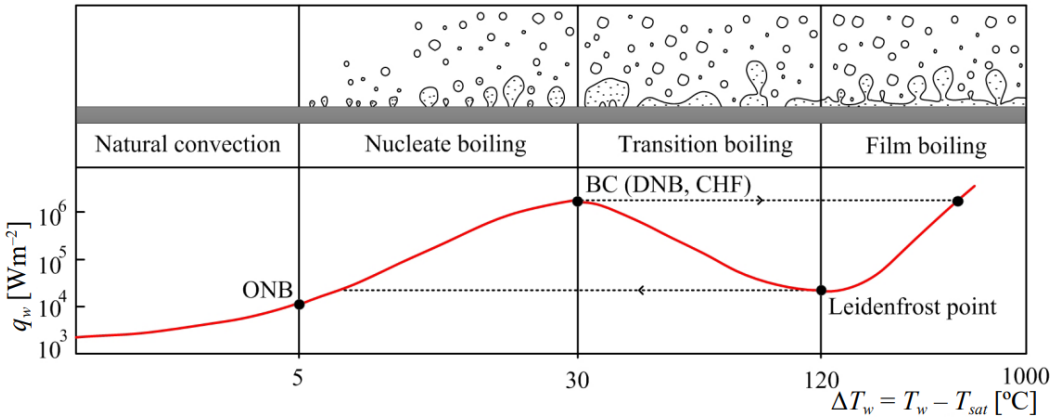

Figure 2.7: Boiling curve obtained from [5]

2.5.1.2 Flow boiling

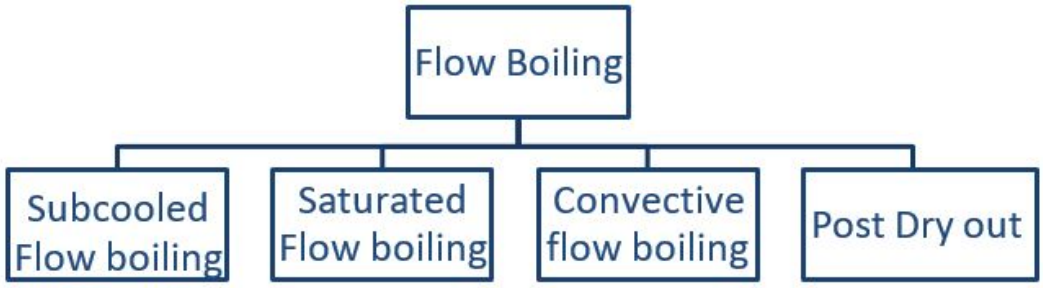

Figure 2.8: Flow boiling

Figure 2.8 gives us the stages of flow boiling in general given by Sarit et.al [6].

- Sub-cooled boiling is referred to as the boiling at the heated wall where the bulk temperature of the liquid is below its saturation temperature. There is one distinctive feature of subcooled boiling. Surface factors (such as surface

roughness) have less of an impact than in pool boiling. This is because, in comparison to pool boiling, the flow requires a higher heat flux, activating a greater number of nucleation sites and decreasing the effect of surface roughness on the process.

- Saturated boiling refers to the boiling where the mean temperature of the liquid reaches the saturation temperature of the liquid at the given temperature. This basically indicates that, according to the thermodynamic equilibrium property, the average enthalpy of the fluid achieves the enthalpy of the saturated fluid. The saturated boiling is in the form of slug or churn flow.

- Following saturated boiling, the vapor slugs gradually become larger and liquid is thrown to the wall, developing into annular flow, which can be observed in Figure 2.9. This region is called convective boiling. This region's unique characteristic is its gradually declining nucleation, which eliminates it nearly entirely downstream. Consequently, evaporation causes the phase shifts to occur here at the vapor–liquid interface.

- When the liquid film in the convective boiling entirely dries up, or, to put it another way, after CHF due to dry out, the heat transfer process takes place. This area involves heat transmission with liquid droplets in vapor, which is the spray flow, cooling the wall as a result of the vapor flow within the tube. This is called "post dry out heat transfer."

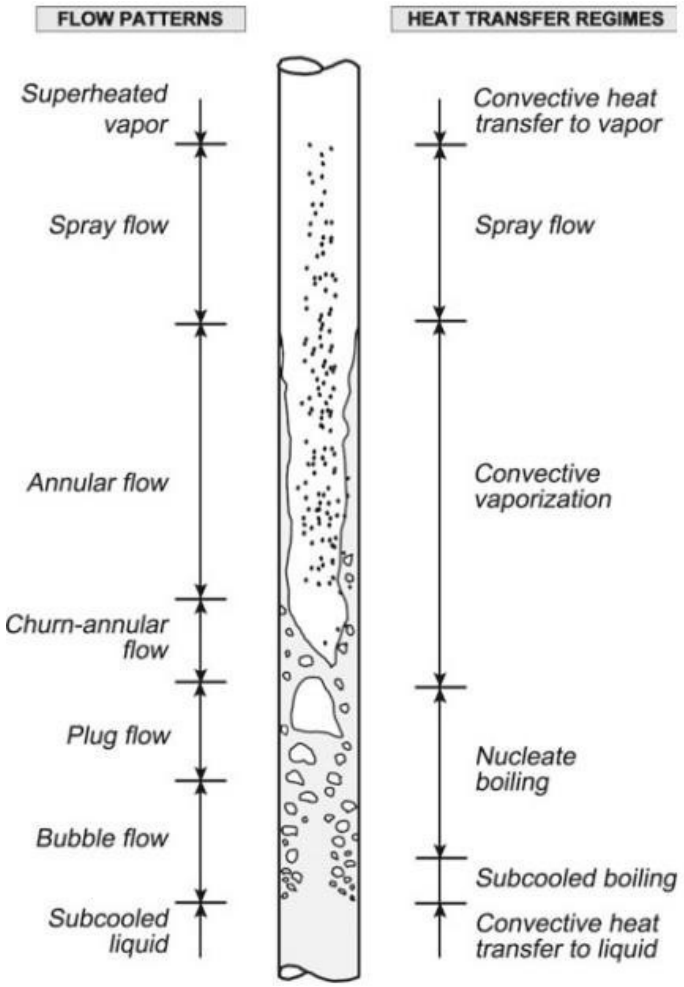

Figure 2.9: Flow pattern [7]

2.5.1.3 Flow Regimes

Figure 2.10 refers to the different regimes in flow boiling through horizontal pipes [8]. The flow starts with liquid, and further along the tube, when the heat flux increases, the wall temperature exceeds the saturation temperature of the liquid, the nucleation of bubbles will be initiated by the cavities and grooves in the heated surface and becomes 'bubbly flow'.

- As the heat flux increases, bubble growth will increase, and after a certain point, the growing bubbles start to coalesce together to form slug and plug flows. These types of flows are called 'Intermittent flows'.
- At high flow rates, the vapor phase will completely cover the upper part of the tube and form a wavy nature. The wavy flow will then become stratified. As the name suggests, the two phases have a clear distinction between them. The gas is always at the top of the tube, and the liquid settles at the bottom of the tube due to the density difference between them.
- Further increase in heat flux makes the flow become annular flow. In this type of flow, the vapor phase is entrapped in the core of the tube and the liquid phase forms a film over the circumference of the tube.

- The mist flow, which can start at the top perimeter where the annular film is the thinnest and move downstream to the bottom perimeter, is reached at very high gas flow rates.

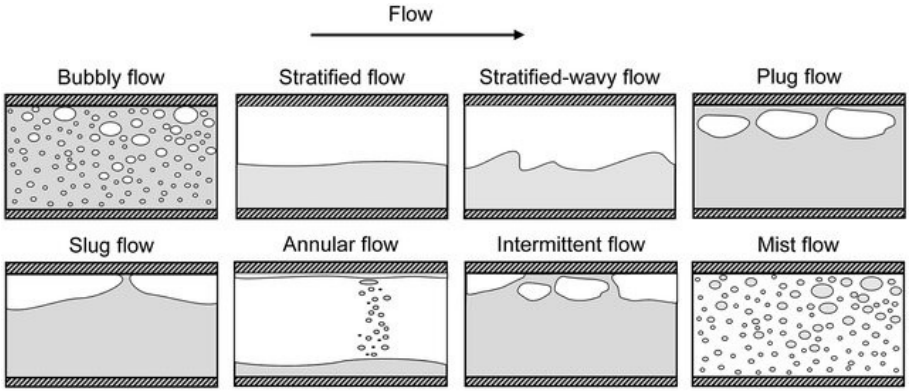

Figure 2.10: Flow boiling regimes [9]

2.5.1.4 Flow Pattern Map

The two main categories of flow-pattern maps are theoretical or semi-theoretical, whose transitions are inferred from physical models of the flow phenomena, and empirical, which are typically fitted to the observed flow-pattern database. The development of theoretical or semi-theoretical flow-pattern maps is based on the flow structure and can occasionally be connected to diabatic properties and heat transmission mechanisms. The surface gas and liquid velocities are two examples of the two flow parameters that are typically used to construct a coordinate system on which the boundaries between the various flow patterns are plotted.

Figure 2.11 gives an empirical flow pattern map which is given by Mandhane, J. M et al [10]. In two-phase flow analysis, a flow pattern map is a graphical depiction that shows the predominant flow patterns under various operating scenarios. With the help of distinct flow patterns, it aids researchers in understanding how the liquid and vapor phases behave in different areas of a flow system. These maps are very helpful for foretelling and depicting the changes in flow regimes. It is to be noted that the empirical flow pattern maps will be valid only for the same working fluid and similar working conditions, and there are numerous flow pattern maps for different working fluids and operating conditions.
The axes in the flow pattern map are the superficial air and water mass flow rates. The superficial velocity of a phase is defined as the velocity of the phase if the other phase was absent and it is defined as,

$$u_s = \frac{Q}{A} \tag{2.16}$$

Where:

- u_s is the superficial velocity of the phase, m/s
- Q is the volume flow rate of the phase, m^3/s
- A is the cross-sectional area, m^2

It can be seen that the map is divided into several regions based on the flow regime that the flow is based on the liquid and vapor velocities. It is observed that the regions namely stratified, annular, plug, and slug are present only for a certain range of superficial liquid and vapor velocities.

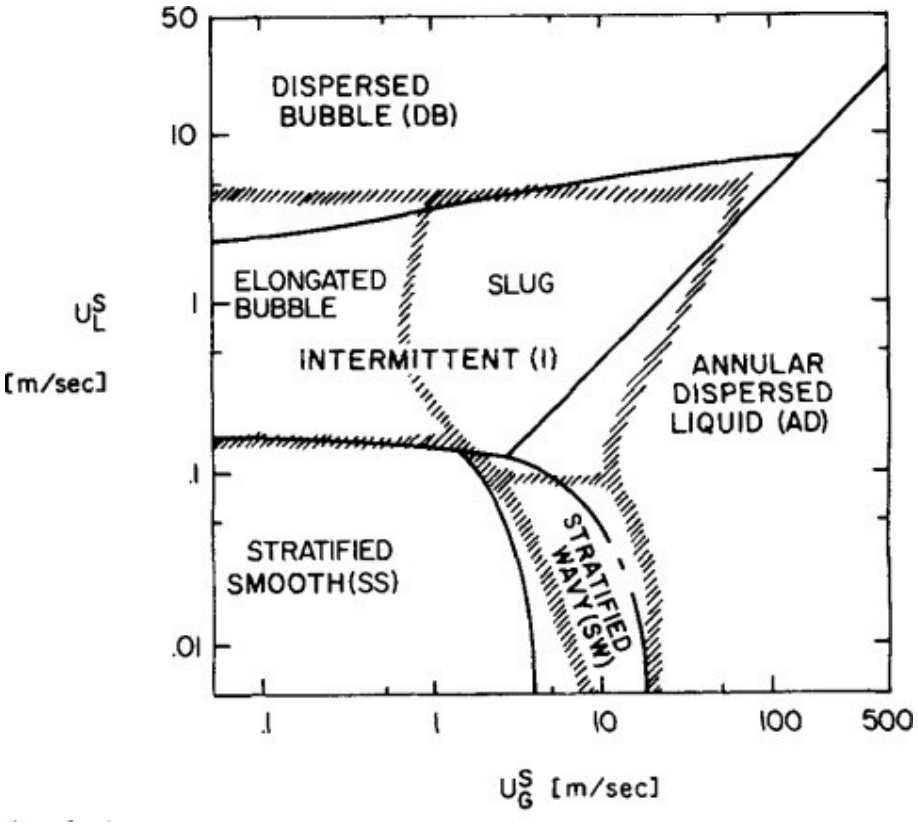

Figure 2.11: Flow pattern map from [11]

2.6 Single Phase Correlations

2.6.1 Pressure Loss Correlations

A fundamental aspect in fluid dynamics and engineering is pressure loss in fluid flow through pipes and channels. The two main causes of pressure loss in single-phase flow, when the fluid is either completely liquid or completely gas, are frictional losses brought on by the fluid's viscosity and losses brought on by modifications in the flow direction or cross-sectional area. Some of the empirical correlations that have been developed to pressure loss are listed below.

2.6.1.1 Darcy-Weisbach Equation

The Darcy-Weisbach equation is one of the most fundamental equations for estimating the pressure loss in a pipe due to friction. The Darcy-Weisbach equation is given by:

$$\Delta P = f \frac{L}{D} \frac{\rho V^2}{2} \tag{2.17}$$

Where:

- ΔP is the pressure drop
- f is the friction factor
- L is the pipe length
- D is the pipe diameter
- ρ is the density of the fluid
- V is the velocity of the fluid

There are various correlations to find the friction factor which are listed below.

2.6.1.2 Moody Friction Factor

The Moody friction factor [12] is denoted by the symbol f and is used in the Darcy-Weisbach equation to calculate the pressure drop due to friction in a pipe. The Moody friction factor for turbulent flows is given as:

$$f = 0.0055 \left[1 + \left(2 \times 10^4 \frac{\epsilon}{D} + \frac{10^6}{Re} \right)^{1/3} \right] \tag{2.18}$$

Where:

- ϵ is the height of surface irregularities

2.6.1.3 Blasius Friction Factor

For hydraulically smooth and turbulent flow in pipes where the Reynolds number is less than 10^5, the friction factor can be approximated by the Blasius formula [13] for finding the friction factor which can be expressed as:

$$f = (0.079\, Re^{-0.25}) \tag{2.19}$$

2.6.1.4 Eckert Friction Factor

An implicit technique for estimating the friction factor for turbulent flow in pipes is the Eckert friction factor approach, commonly referred to as the Eckert correlation [14].
The Eckert friction factor is expressed as:

$$\frac{1}{\sqrt{f}} = -2 \log \left(\frac{\epsilon/D}{3.715} + \frac{15}{Re} \right) \tag{2.20}$$

2.6.2 Heat Transfer Correlations

Heat transfer correlations for single-phase flow are empirical relationships which are derived from experimental data or theoretical analysis to estimate the heat transfer under different flow conditions. Here are some common heat transfer correlations for single-phase flow:

2.6.2.1 Dittus-Boelter

The Dittus-Boelter equation [15] is a popular correlation which is widely used for finding the local Nusselt number in a fully developed (both hydrodynamically and thermally) turbulent flow in a smooth pipe. It is generally more suitable for flows with small to moderate temperature difference between the wall and the fluid. The Dittus-Boelter equation is expressed as:

$$Nu_{D_h} = 0.023\, Re_{D_h}^{0.8}\, Pr^{0.4} \tag{2.21}$$

Where:

- D_h is the hydraulic diameter, m
- Nu is the Nusselt number
- Pr is the Prandtl number
- Re_{D_h} is the Reynolds number

2.6.2.2 Sieder-Tate

The Sieder-Tate equation [16] which was proposed by Sieder and Tate in 1936 is a modified version of the Dittus-Boelter equation. The addition in this equation is the consideration of the viscosity variation with temperature which is important for flows with high temperature difference between the surface and the fluid. The Sieder-Tate correlation is given by:

$$Nu_{D_h} = 0.027\, Re_{D_h}^{0.8}\, Pr^{0.33} \left(\frac{\mu}{\mu_s}\right)^{0.14} \tag{2.22}$$

2.6.2.3 Gnielinski

Even though the above-mentioned correlations can be easily applied, there can be 25% error between the correlations and experimental results. These errors can be reduced by the usage of more recent correlations which are said to be more accurate. The Gnielinski correlation [17] is valid for a wide range of Reynolds numbers, even including the transition regime. The equation is expressed as:

$$Nu_{D_h} = \frac{f/8(Re_{D_h} - 1000)Pr}{1 + 12.7(f/8)^{1/2}(Pr^{2/3} - 1)} \tag{2.23}$$

2.7 Two-Phase Correlations

Two-phase correlations are empirical or semi-empirical relationships used to predict the behavior of fluid flow and heat transfer in systems where two phases (usually liquid and vapor) coexist. The key parameters typically addressed by two-phase correlations include pressure drop and heat transfer coefficient.

2.7.1 Pressure Drop Correlations

The pressure drop that happens when a two-phase flow goes through a pipe or a system is estimated using two-phase pressure loss correlations. In many technical applications, such as the design and analysis of heat exchangers, these correlations are crucial.

2.7.1.1 Lockhart-Martinelli Correlation

The Lockhart and Martinelli method [18] for predicting the two-phase pressure drop is the method published in 1949. The two-phase frictional pressure drop is estimated based on a two-phase multiplier for the liquid phase or the vapor phase respectively as:

$$\Delta p_{\text{fric}} = \phi^2 \frac{\Delta p_L}{\mathrm{L_{tt}}} \quad \text{or} \quad \Delta p_{\text{fric}} = \phi_{\text{tt}}^2 \frac{\Delta p_G}{G} \tag{2.24}$$

Where Δp_L and Δp_G are the pressure drop for each phase which are given as:

$$\Delta p_L = 4 f_L \left(\frac{L}{d}\right) \dot{m}^2 \left(1 - x^2\right) \left(\frac{1}{2}\rho\right) \tag{2.25}$$

$$\Delta p_G = 4 f_G \left(\frac{L}{d}\right) \dot{m}^2 \left(x^2\right) \left(\frac{1}{2}\rho\right) \tag{2.26}$$

Where:

- f_L and f_G are the single-phase frictional factors of the liquid and the vapor phase
- d is the inner diameter of the pipe
- L is the length of the pipe
- ρ_L and ρ_G are the densities of the liquid and vapor phase respectively
- $\dot{m}_{\text{total}}$ is the total mass velocity
- x is the vapor quality
- Re is the Reynolds number

The corresponding two-phase multipliers are expressed as:

$$\phi^2 = 1 + \frac{C + 1}{\mathrm{L_{tt}}} \quad \text{for} \quad Re > 4000 \tag{2.27}$$

$$\phi^2 = 1 + C_{\text{tt}} \mathrm{L_{tt}} + \mathrm{L_{tt}^2} \quad \text{for} \quad Re_L < 4000 \tag{2.28}$$

Where:

- $\mathrm{L_{tt}}$ is the Martinelli parameter
- C is a constant depending on the regimes both the phases are in and it is given in table 2.1

The Lockhart-Martinelli correlation is one of the simplest and useful correlations used for predicting pressure loss among the other correlations.

Liquid	Vapor	C
Turbulent	Turbulent	20
Laminar	Turbulent	12
Turbulent	Laminar	10
Laminar	Laminar	5

Table 2.1: Constant conditions

2.7.1.2 Chisholm Correlation

Chisholm in 1973 proposed an extensive method [19] empirically which is applicable to a wide range of operating conditions compared to Lockhart-Martinelli. The two-phase frictional pressure drop gradient by Chisholm is given as:

$$\Delta p_{\text{fric}} = \phi^2 \frac{\Delta p_L}{C_h} \tag{2.29}$$

The frictional pressure gradients for the liquid and vapor phases can be:

$$\Delta p_L = 2 f_L \frac{\dot{m}^2_{\text{liquid}}}{\rho_L L d} \tag{2.30}$$

$$\Delta p_G = 2 f_G \frac{\dot{m}^2_{\text{vapor}}}{\rho_G L d} \tag{2.31}$$

The frictional factors can be calculated using the same equations as Lockhart-Martinelli. Chisholm's two-phase multiplier can be expressed as:

$$\phi^2 = 1 + (Y^2 - 1)\left[\frac{B_x}{2} + x^{2-n}\right] \tag{2.32}$$

Where:

- Y is the ratio of the frictional pressure gradients and is given as

$$Y^2 = \frac{\Delta p_G}{\Delta p_L} \tag{2.33}$$

- B is called the Chisholm's parameter and it can be calculated as follows:
  - When $0 < Y < 9.5$:

$$B = \begin{cases} 55 & \text{for } \dot{m}_{\text{total}} > 1900\,\text{kg/s} \\ 2400 & \text{for } 500 < \dot{m}_{\text{total}} < 1900\,\text{kg/s} \\ 4.8 & \text{for } \dot{m}_{\text{total}} < 1900\,\text{kg/s} \end{cases} \tag{2.34}$$

  - When $9.5 < Y < 28$:

$$B = \begin{cases} 520 & \text{for } \dot{m}_{\text{total}} < 600\,\text{kg/s} \\ \frac{\dot{m}_{\text{total}}}{Y} & \text{for } 600\,\text{kg/s} < \dot{m}_{\text{total}} < 1900\,\text{kg/s} \end{cases} \tag{2.35}$$

  - When $Y > 28$:

$$B = \frac{15000}{Y^2 \dot{m}^2_{\text{total}} \text{to}} \tag{2.36}$$

The Chisholm correlation is one of the versatile methods with improved accuracy and is said to be applicable for a wide range of operating conditions.

2.7.2 Heat transfer correlations

In engineering applications where both liquid and vapor phases are present concurrently, as in processes like boiling and condensation, heat transfer correlations for two-phase flow are essential. By establishing links between flow parameters, thermodynamic properties, and heat transfer coefficients, these correlations enable accurate predictions of heat transfer rates across a range of applications.

2.7.2.1 Chen correlation

The Chen correlation [20] for the boiling heat transfer coefficient, published in 1990, has been used for several years for water flowing through tubes. This correlation was the very first to use the superposition approach of nucleation and forced convection mechanisms. The Chen correlation can be expressed as,

$$\begin{aligned} h = 0.00122 \left(\frac{{K_l}^{0.79} {C_{pl}}^{0.45} {\rho_l}^{0.49}}{{\mu_l}^{0.29} \sigma^{0.5} {i_{fG}}^{0.24} {\rho_v}^{0.24}} \right) {\Delta T_{sat}}^{0.24} {\Delta P_{sat}}^{0.75} S \\ +0.023 \left[\frac{G(1-x_z)D}{\mu_L} \right]^{0.8} \left[\frac{\mu_L C_p}{K_L} \right]^{0.4} \frac{K_l F}{D} \end{aligned} \tag{2.37}$$

Where:

K is the thermal conductivity,
L is the length of the tube,
D is the diameter of the tube,
C_p is the specific heat,
ρ is the density,
σ is the surface tension,
μ is the viscosity,
ΔT_{sat} is the wall superheat,
Δp_{sat} is the saturation pressure difference between the wall and bulk temperatures,
G is the mass flux,
x is the local vapor quality,
i_{fG} is the latent heat of vaporization.

The parameter S in Equation 2.37 can be calculated as

$$S = \frac{1}{1 + 2.53 \times 10^{-6} F^{1.25} \frac{G(1-x)}{D/\mu_L}} \tag{2.38}$$

And in this equation, the parameter F can be calculated as

$$F = \begin{cases} 1 & \text{if } \chi_{tt} < 0.1 \\ \frac{1}{2.35} \left(\frac{1}{\chi_{tt}} + 0.213 \right) & \text{if } \chi_{tt} > 0.1 \end{cases} \tag{2.39}$$

Where χ_{tt} is the Lockhart-Martinelli parameter defined in Section 2.7.1.1.

The Chen correlation is particularly useful for predicting heat transfer in boiling systems where both nucleate and forced convection are significant. The correlation is said to produce reliable predictions for low to moderate heat fluxes and operating pressures. However, the correlation assumes a relatively uniform flow distribution and therefore may not account for dryout or film boiling.

2.7.2.2 Modified Tran correlation

The modified Tran correlation was given by Yu [21]. The original Tran heat transfer correlation [22] was developed for refrigerants, but the modified Tran correlation is for water as its working fluid. The modified Tran correlation is given as,

$$h = 6400000 \left(Bo^2 We\right)^{0.27} \frac{\rho_l^{-0.2}}{\rho_g} \tag{2.40}$$

Where:

Bo is the boiling number and is given as

$$Bo = \frac{q}{Gh_{LG}},$$

We is the Weber number and is given as

$$We = \frac{G^2 D}{\sigma \rho_l},$$

ρ_g and ρ_l are the densities of the vapor and liquid respectively.

2.7.2.3 Liu and Winterton correlation

The Liu and Winterton correlation, proposed by Z. Liu and R.H.S. Winterton in 1990 [23], gave a predictive method for heat transfer by covering a wide range of parameters and an explicit nucleate boiling term. The explicit method for nucleate boiling was adapted to better predict the applications relating to subcooled boiling. The Liu and Winterton correlation is given as,

$$h_{tp} = \sqrt{(Fh_{fc})^2 + (Sh_{pb})^2} \quad \text{(saturated boiling)} \tag{2.41}$$

$$h_{tp} = \sqrt{(Fh_{fc})^2 + (Sh_{pb}(T_w - T_b))^2} \quad \text{(subcooled boiling)} \tag{2.42}$$

Where:

- h_{tp} is the two-phase flow heat transfer.
- h_{fc} is the heat transfer due to forced convection and is given by

$$h_{fc} = 0.023 Re_l^{0.8} Pr_l^{0.4} \frac{k_l}{D_{in}} \tag{2.43}$$

where Re_l is the liquid Reynolds number, Pr_l is the liquid Prandtl number, k_l is the liquid thermal conductivity, and D_{in} is the inner diameter.

- h_{pb} is the heat transfer due to pool boiling and is given by

$$h_{pb} = 55 \left(\frac{P_{cr}^{0.12}}{P^{0.12}} \right) \left[-\log_{10} \left(\frac{P}{P_{cr}} \right) \right]^{-0.55} M^{-0.5} q^{0.67} \tag{2.44}$$

  where P_{cr} is the critical pressure, P is the pressure, q is the heat flux, and M is the molecular weight.
- F is the forced convection heat transfer enhancement factor and is given by

$$F = \frac{0.35}{\rho_l} \left(1 + x_e Pr_l(\rho_v - 1)\right) \tag{2.45}$$

  where x_e is the exit vapor quality, ρ_l is the liquid density, and ρ_v is the vapor density.
- S is the suppression factor and is given by

$$S = \frac{1}{1 + 0.055 F^{0.1} Re_l^{0.16}} \tag{2.46}$$

The Liu and Winterton correlation, unlike the Chen correlation, is applicable for a wider range of heat fluxes and operating pressures, making it a preferred choice in various engineering applications.

2.7.3 Previous experimental studies

The literature study mainly focused on experiments with horizontal pipes with diameters closely matching those of the heat exchanger pipes in the engine of interest. Another important aspect considered was the working fluid, which is water for our heat exchangers. With respect to experiments on flow boiling of water in horizontal flows, there are only a handful of experiments available.

- **Yu et al.** [21] studied the two-phase pressure drop, boiling heat transfer, and critical heat flux of water flowing through a horizontal tube with a diameter of 2.98mm. The tests were conducted for varying mass fluxes and heat fluxes. The results of pressure drop were compared against the Chisholm correlation, and a modification of the correlation was provided based on the empirical results from the experiment. The Chisholm multiplier was changed from,

$$\varphi^2 = 1 + C + \frac{1}{F_L}$$

  And it was changed to

$$\varphi^2 = X^{-1.9}$$

  The proposed change in the Chisholm correlation was observed to have only 7% deviation between the results from the original of 33% deviation. In addition, comparison of heat transfer coefficient with the Chen correlation which was found to have 30% deviation with the experiments. In addition, the paper compares the critical heat flux between the experiments and a predictive method given by Groeneveld-Cheng-Doan [24] and the critical heat flux was found to occur at higher vapor qualities between 0.5 and 1.0.

- **Hardik et al.** [25] investigated the heat transfer and pressure drop in flow boiling of water in horizontal tubes at low pressure. The effect of tube diameter, system pressure, heating length, mass flux, and heat flux on pressure drop and heat transfer was studied. The experimental results obtained were compared with a number of correlations for both pressure drop and heat transfer, and a new correlation was developed for pressure drop from the obtained experimental results where the Chisholm multiplier (C) was modified from the value 20 for turbulent-turbulent flow to,

  $$C = 18e^{0.14d}$$

  The updated Chisholm multiplier showed a 20% deviation compared to the original deviation of 40%. It was found that the boiling heat transfer coefficient is not dependent on tube diameter, while tube diameter has a higher influence on two-phase pressure drop.

Apart from experimental studies on water, there are also studies on refrigerants.

- **Wojtan et al.** [8] developed a new predictive method for heat transfer by making modifications to the original heat transfer model by Kattan et al [26]. The new approach showed a good improvement in predicting heat transfer, even at lower vapor qualities.
- **Han et al.** [27] analyzed the boiling heat transfer coefficient of R134a flowing in a 5mm inner diameter smooth horizontal tube. It was observed that for increasing pressures, the location of the maximum heat transfer coefficient shifts to lower vapor qualities. The heat transfer prediction of Wojtan et al. was compared with experimental results, showing good agreement up to 0.7 vapor quality, but increasing deviation near dryout conditions.
- **Jige et al.** [28] investigated the flow boiling characteristics of refrigerant R32 for different diameters, mass fluxes, and heat fluxes. The experimental values of pressure drop and heat transfer coefficient were compared with empirical correlations, including the work of Yu et al. It was found that nucleate boiling heat transfer was dominant under high heat flux and lower vapor quality conditions.

From the understanding of the experimental studies done previously, the experiment done by Yu seems to be the experiment that closely matches with the requirements that is required. The experiments are done in horizontal tubes with a tube diameter closer to the heat exchangers of interest along with the working fluid as water. The experiment also has the working conditions such as the liquid is in laminar condition at the inlet such as the heat exchanger's condition of interest. In addition, the experiments compare the results with correlations to give the idea of how accurate the correlations to the experimental results.

3

Computational Fluid Dynamics

Within the discipline of fluid mechanics, computational fluid dynamics (CFD) combines numerical techniques and algorithms to analyzing and resolving of fluid flow-related problems. It involves replicating fluid flow behavior and how it interacts with solid structures with the help of computers. Many industries in engineering employ the use of CFD to analyze and improve the performance of fluid-moving systems.
Primarily, Computational Fluid Dynamics (CFD) solves the Navier-Stokes equation which are in general a set of partial differential equations that expresses the fluid motion. The following details about the models are obtained from the ANSYS theory guide [29] . For an incompressible flow problem, the Navier-Stokes equations are expressed in the following section.

3.1 Conservation of Mass

The conservation of mass or the Continuity equation is one of the fundamental equations in fluid mechanics. In a confined region, it explains how the fluid mass is conserved. The Continuity equation solved by Fluent 2023r1 is expressed as

$$\frac{\partial \rho}{\partial t} + \nabla \cdot (\rho \mathbf{v}) = S_m \tag{3.1}$$

Where S_m is the mass added to the continuous phase from the dispersed secondary phase, for example, vaporization of liquid droplets.

3.2 Conservation of Momentum

The conservation of momentum, or commonly known as the Navier-Stokes equation in Fluent 2023r1, is expressed as

$$\frac{\partial (\rho \mathbf{v})}{\partial t} + \nabla \cdot (\rho \mathbf{v} \times \mathbf{v}) = -\nabla P + \nabla \cdot (\tau) + \rho \mathbf{g} + \mathbf{F} \tag{3.2}$$

Where

- $\mathbf{g}$ is the gravitational force
- $\mathbf{F}$ is the external body forces
- τ is the stress tensor, given by

$$\tau = \mu \left[\left(\nabla \mathbf{v} + \nabla \mathbf{v}^T \right) - 2 \nabla \cdot \mathbf{v} \mathbf{I} \right] \tag{3.3}$$

Where μ is the molecular viscosity, $\mathbf{I}$ is the unit tensor, and the second term on the right-hand side is the effect of volume dilation.

3.3 The Energy Equation

The energy equation is solved in the following form in Fluent 2023r1:

$$\frac{\partial}{\partial t}\left[\rho\left(e+\frac{v^2}{2}\right)\right]+\nabla\cdot\left[\rho\mathbf{v}\left(h+\frac{v^2}{2}\right)\right]=\nabla\cdot\left(k_{eff}\nabla T-\sum_j \mathbf{J}_j\cdot\mathbf{h}_j+\tau_{eff}\cdot\mathbf{v}\right)+S_h \tag{3.4}$$

Where

- k_{eff} is the effective thermal conductivity ($k+k_t$ where k_t is the turbulent thermal conductivity defined by the turbulence model used and k is the molecular thermal conductivity)
- e is the internal energy
- h is the enthalpy
- ρ is the density
- $\sum_j \mathbf{J}_j\cdot\mathbf{h}_j$ is the species diffusion
- $\tau_{eff}\cdot\mathbf{v}$ is the viscous dissipation
- S_h includes the volumetric heat sources that have been defined and the heat generation rate from chemical reactions.

The enthalpy h is defined as:

$$h=\sum_j Y_j h_j \tag{3.5}$$

Where Y_j is the mass fraction of species j and the enthalpy of species h_j is defined as:

$$h_j=\int_{T_{ref}}^{T} c_{p,j}dT \tag{3.6}$$

For the pressure-based solver, T_{ref} is 298.15K.

3.4 Turbulence Modelling

When the fluid flow becomes turbulent, it exhibits chaotic behavior, making it very difficult to solve the equations mentioned above. To model this turbulent flow behavior, Reynolds Averaged Navier Stokes (RANS) equations are used in CFD. The Reynolds averaging technique is applied to the Navier-Stokes equations, separating the components into mean and fluctuating components.
The velocity components can be expressed as:

$$u_i=\overline{u}_i+u_i' \tag{3.7}$$

Where $\overline{u}_i$ and u_i' denote the mean and fluctuating components, respectively. Other scalar quantities can be expressed likewise:

$$\phi_i=\overline{\phi}_i+\phi_i' \tag{3.8}$$

Substituting these expressions into the instantaneous equations of continuity and momentum equations and time averaging yields the RANS equations.

RANS Continuity Equation

$$\frac{\partial \rho}{\partial t} + \frac{\partial (\rho u_i)}{\partial x_i} = 0 \tag{3.9}$$

RANS Momentum Equation

$$\begin{aligned} \frac{\partial (\rho u_i)}{\partial t} + \frac{\partial (\rho u_i u_j)}{\partial x_j} = &- \frac{\partial p}{\partial x_i} + \frac{\partial}{\partial x_j}\left(\mu\left(\frac{\partial u_i}{\partial x_j} + \frac{\partial u_j}{\partial x_i} - \frac{2}{3}\frac{\partial u_l}{\partial x_l}\delta_{ij}\right)\right) \\ &+ \frac{\partial}{\partial x_j}\left(-\rho \overline{u}_i \overline{u'_j}\right) \end{aligned} \tag{3.10}$$

Where:

- $\overline{u}_i \overline{u}'_j$ represents the Reynolds stresses which represent the fluctuating component of the momentum transport due to turbulent eddies.

Reynolds stresses, which reflect the extra momentum transport brought on by turbulent variations, are essential to the modeling of turbulent flow. They are commonly included in turbulence models used in computational fluid dynamics (CFD) simulations because they are crucial for precisely forecasting the behavior of turbulent flows.

3.4.1 Eddy Viscosity Models

A common method used to model the Reynolds stresses employs the Boussinesq hypothesis that relates the Reynolds stresses to the mean velocity gradients.

$$-\overline{\rho u'_i u'_j} = \mu_t \left(\frac{\partial u_i}{\partial x_j} + \frac{\partial u_j}{\partial x_i}\right) - 2\left(\rho k + \mu \frac{\partial u_k}{\partial x_k}\right)\delta_{ij} \tag{3.11}$$

Where:

- μ_t is the turbulent eddy viscosity
- δ_{ij} is the Kronecker delta

The Boussinesq hypothesis can be used in $k-\varepsilon$ and $k-\omega$ turbulence models which are explained below.

3.5 k-ε Model

One of the most widely used turbulence models in the simulation of turbulent flows is the k-ε turbulence model proposed by Launder & Spalding [30]. This model solves transport equations for the turbulent kinetic energy (k) and turbulent dissipation rate (ε).

Turbulent Kinetic Energy (k)

$$\frac{\partial (\rho k)}{\partial t} + \frac{\partial (\rho u_i k)}{\partial x_i} = \frac{\partial}{\partial x_j}\left[\left(\mu + \frac{\mu_t}{\sigma_k}\right)\frac{\partial k}{\partial x_j}\right] + G_k + G_b - \rho\varepsilon + S_k \tag{3.12}$$

Where:

- k is the turbulent kinetic energy
- ρ is the density
- G_k is the production of turbulent kinetic energy due to mean velocity gradients
- G_b is the production of turbulent kinetic energy due to buoyancy
- S_k is the user-defined source term
- μ_t is the turbulent viscosity
- σ_k is the turbulent Prandtl number

Turbulent Dissipation Rate (ε)

$$\frac{\partial(\rho\varepsilon)}{\partial t} + \frac{\partial(\rho u_i \varepsilon)}{\partial x_i} = \frac{\partial}{\partial x_j}\left[\left(\mu + \frac{\mu_t}{\sigma_\varepsilon}\right)\frac{\partial \varepsilon}{\partial x_j}\right] + C_{\varepsilon 1}\left(G_k + C_{\varepsilon 3} G_b\right) - C_{\varepsilon 2}\rho\frac{\varepsilon^2}{k} + S_\varepsilon \tag{3.13}$$

Where:

- $C_{\varepsilon 1}$, $C_{\varepsilon 2}$, and $C_{\varepsilon 3}$ are model coefficients specific to the chosen k-ε model
- G_ε is the production of turbulent dissipation due to mean velocity gradients
- S_ε is the user-defined source term

The turbulent viscosity μ_t is computed using k and ε as follows:

$$\mu_t = C_\mu \frac{\varepsilon}{k} \tag{3.14}$$

In Fluent 2023r1, the default value for C_μ is 0.09.

3.6 k-ω SST Model

One common hybrid turbulence model used in computational fluid dynamics (CFD) simulations is the k-ω SST (Shear Stress Transport) model proposed by Menter [31]. It provides better predictions for a variety of flow scenarios, such as boundary layer, separated, and unfavorable pressure gradient flows by combining the superior performance of the k-ε model in the free stream and k-ω model near the walls.

Turbulent Kinetic Energy (k)

The turbulent kinetic energy (k) is obtained using an equation similar to the standard k-ε model.

$$\frac{\partial k}{\partial t} + U_j \frac{\partial k}{\partial x_j} = \frac{\partial}{\partial x_j}\left[\left(\nu + \sigma_k \nu_t\right)\frac{\partial k}{\partial x_j}\right] - \beta^* k\omega + G_k + G_b + S_k \tag{3.15}$$

Specific Dissipation Rate (ω)

$$\frac{\partial \omega}{\partial t} + U_j \frac{\partial \omega}{\partial x_j} = \frac{\partial}{\partial x_j}\left[\left(\nu + \sigma_\omega \nu_t\right)\frac{\partial \omega}{\partial x_j}\right] - \beta\omega^2 + \alpha S^2 + 2(1 - F_1)\sigma_\omega^2 \tag{3.16}$$

Where:

- ν is the kinematic viscosity
- ν_t is the kinematic eddy viscosity

- U_j is the strain rate
- F_1 and F_2 are the closure coefficients
- S is the strain rate magnitude
- β, β^*, σ_k, and σ_ω are model constants

The effective diffusivities of the k-ω model in Fluent 2023r1 are given as:

$$\begin{aligned} \mu_t \Gamma_k &= \mu + \sigma_k k \\ \mu_t \Gamma_\omega &= \mu + \sigma_\omega \omega \end{aligned} \tag{3.17}$$

The turbulent viscosity, μ_t, is computed by combining k and ω as:

$$\mu_t = \frac{k}{\omega} \tag{3.18}$$

3.7 Multiphase Models

The term "multiphase flow" describes the simultaneous movement of several phases of matter—such as liquids, gases, or solids—within a single domain. CFD software offers a variety of multiphase flow models tailored to address several multiphase flow scenarios. To accurately simulate complicated flow processes involving interactions between many phases, such as liquids, gases, and solids, multiphase models must be used. By considering the distinct characteristics and behaviors of each phase—a vital component in the prediction of heat and mass transfer, phase interactions, and general flow patterns—these models improve the accuracy of simulations.
Among the most popular of these models are:

3.7.1 Volume of Fluid (VOF)

The VOF model tracks the volume fractions of different fluid phases within each computational cell. It uses an interface capturing technique to describe the interface between phases, where the interface is tracked across one or more grid cells. The VOF model is particularly useful in problems where the position and shape of the interface between fluids are important and need to be accurately captured.
The VOF model's volume fraction transport equation is solved in conjunction with the Navier-Stokes equations for momentum and the continuity equation. The resulting solution provides detailed information about the location and shape of the interface between the fluids over time, allowing for accurate simulations of complex multiphase flow phenomena. The volume fraction's advection, diffusion, and phase change are all governed by this equation. Within each cell, the volume fractions of all phases add up to unity.
The volume fraction equation for the qth phase is given in the form,

$$\frac{1}{\rho_q}\frac{\partial(\alpha_q \rho_q)}{\partial t} + \nabla \cdot (\alpha_q \rho_q \mathbf{v}_q) = S_{\alpha_q} + \sum_{p=1}^{n}(\dot{m}_{pq} - \dot{m}_{qp}) \tag{3.19}$$

Where:

- $\dot{m}_{pq}$ is the mass transfer from phase p to phase q

- $\dot{m}_{qp}$ is the mass transfer from phase q to phase p
- S_{α_q} is the source term
- α_q is the volume fraction of phase q

3.7.2 The Mixture Model

A method for simulating multiphase flows in which the phases are interpenetrating but still distinct despite being blended on a smaller scale is called the mixture model. This model is especially helpful for flows with phases that have different characteristics but comparable velocities, like bubbly, slurry, and particle-laden flows. Compared to fully resolved multiphase models such as the Eulerian-Eulerian model, the mixture model is computationally less expensive because it reduces the complexity of multiphase flow by employing a single set of governing equations for the mixture. The mixture model makes the assumption that the phases move at comparable speeds, which could not be true for all kinds of multiphase flows, particularly when there is a lot of interphase slip.
The volume fraction equation that is solved in the mixture model for phase p is given as,

$$\frac{\partial(\alpha_p\rho_p)}{\partial t} + \nabla\cdot(\alpha_p\rho_p\mathbf{v}_m) = -\nabla\cdot(\alpha_p\rho_p\mathbf{v}_{dr,p}) + \sum_{q=1}^{n}(\dot{m}_{pq} - \dot{m}_{qp}) \tag{3.20}$$

Where:

- $\mathbf{v}_m$ is the mass averaged velocity
- $\mathbf{v}_{dr,p}$ is the drift velocity for secondary phase p:
  - $\mathbf{v}_{dr,p} = \mathbf{v}_p - \mathbf{v}_m$

3.7.3 Eulerian-Eulerian

The multiphase Eulerian-Eulerian model is a strong and adaptable method for modeling the behavior of several interpenetrating phases. Each phase is viewed as an interpenetrating continuum in the Eulerian-Eulerian model, which has its own unique sets of conservation equations for mass, momentum, and energy. This makes it possible to depict the dynamics of each phase in great detail. The intricacy of representing interphase interactions and the requirement to solve numerous sets of conservation equations make the Eulerian-Eulerian model computationally demanding.
Volume fractions of each phase are incorporated into the description of multiphase flow as interpenetrating continua. Each phase independently satisfies the rules of conservation of mass and momentum, and volume fractions show the space occupied by each phase.
The volume of phase q, V_q, is defined as

$$V_q = \int \alpha_q dV \tag{3.21}$$

Where

$$\sum \alpha_q = 1 \tag{3.22}$$

The effective density of phase q is:

$$\hat{\rho}_q = \alpha_q \rho_q \tag{3.23}$$

Where ρ_q is the physical density of phase q.

3.8 Computational Mesh

The discretization of the computational domain into cells is referred to as the mesh in ANSYS Fluent 2023r1. The quality and effectiveness of the numerical simulations carried out in Fluent 2023r1 are directly impacted by the meshing method, which makes it essential knowledge. The Finite Volume Method (FVM), which is a numerical technique in solving partial differential equations, is the main technique used by ANSYS Fluent 2023r1 to solve fluid flow and heat transfer problems. The computational domain is discretized using this method into control volumes. After integrating the governing equations across these control volumes, algebraic equations with numerical solutions are produced.

3.8.1 Types of Mesh

There are a couple of types of mesh available for discretizing the computational domain. They are structured, unstructured, and hybrid meshes which are shown in Figure 3.1.

3.8.1.1 Structured Mesh

In structured meshes, the computational domain is divided into a grid of cells with a regular and uniform arrangement. The grid cells consist of an orderly arrangement in a regular pattern, either as hexahedra in 3D or rectangles in 2D. Structured meshes are easy to generate and work well for simpler geometries. However, generating structured meshes for complex geometries can be challenging and may require techniques such as block-structured meshing or multi-block meshing. Structured meshes often allow for more efficient numerical computations and memory usage due to their regular arrangement. This can lead to faster solution times and reduced computational costs compared to unstructured meshes.

3.8.1.2 Unstructured Mesh

In contrast to structured meshes, unstructured meshes are more adaptable and flexible. Unstructured meshes enable improved resolution of intricate geometries and flow characteristics because cells can have any size and shape. Algorithms that may adaptively improve the mesh based on geometric complexity or flow gradients are used to build unstructured meshes. They work well with extremely irregular geometries, as those seen in sophisticated industrial equipment, turbomachinery, and automobile components. When it comes to capturing boundary layer effects and resolving flow phenomena like vortices and separation zones, unstructured meshes provide more freedom.

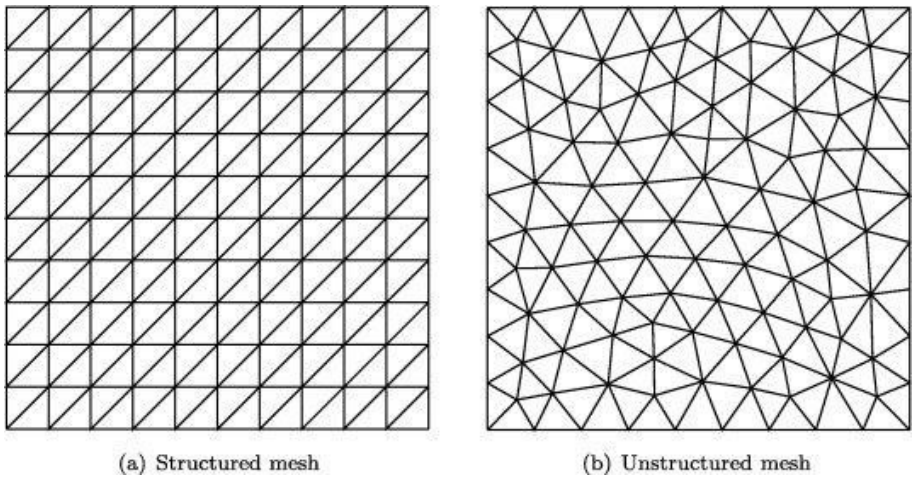

Figure 3.1: Mesh types [32]

3.8.1.3 Hybrid Mesh

A computational grid that incorporates various element types into a single mesh is known as a hybrid mesh. This method improves the accuracy and efficiency of the simulation by utilizing the benefits of several mesh types to better capture intricate geometries and flow aspects. When dealing with situations with complicated borders or when different sections of the flow field require varying levels of resolution, hybrid meshes are especially helpful.

3.8.2 Meshing Techniques

Wall functions and low Reynolds number (Re) meshing techniques are used to accurately capture flow near solid boundaries, especially in regions where the viscous effects dominate which is depicted in Figure 3.2.

3.8.2.1 Wall Function Mesh

In CFD simulations, wall functions are used to define the near-wall flow without explicitly solving the boundary layer. Viscosity effects cause considerable changes in the velocity and turbulence characteristics near solid boundaries, such as walls in a flow domain. Wall functions extend the flow characteristics from neighboring cells into the viscous sub-layer and buffer layer close to the wall, offering a more straightforward way to simulate these alterations. Their foundation lies on empirical correlations that are obtained from both theoretical analyses of boundary layer flow and experimental data. In turbulent flows, wall functions are frequently employed since the mesh close to the wall might not be fine enough to resolve the near-wall turbulence structures and the viscous sub-layer. Wall functions allow one to use coarser meshes away from the wall and yet achieve correct results in the bulk flow region, hence saving computational resources. Wall functions, however, have their limitations and might not be appropriate for flows near walls that have complex flow patterns, separation, or severe adverse pressure gradients.

Wall functions were initially developed for high-Reynolds number turbulence models which become invalid in the laminar part of the turbulent boundary layer. Standard wall functions were derived from the turbulent Couette flow. It can be shown that in the absence of pressure gradients, the non-dimensional tangential velocity and distance to the wall are expressed as:

$$u^+ = \frac{u}{u_\tau} \quad \text{and} \quad y^+ = \frac{y u_\tau}{\nu}$$

Where:

- ν is the kinematic viscosity
- u_τ is the wall shear stress

3.8.2.2 Low Reynolds Number Mesh

Low Reynolds number (Re) meshing is used to resolve flows where viscous effects predominate, which are usually at low velocities or in short length-scale regions. Low Reynolds numbers result in laminar or transitional flow characteristics because viscous forces are comparatively more important than inertial forces. Low Re meshing aims to resolve viscous issues and precisely capture the boundary layer by fine-tuning the mesh in close proximity to solid boundaries. To properly resolve the boundary layer thickness and capture velocity gradients, this usually calls for the usage of finer mesh elements near walls. For precise simulation of laminar or transitional flows, complex boundary layer structures, or separation events, low Reynolds number meshing is required. However, since smaller meshes demand more computer resources, low Re meshing may result in higher computational costs, particularly for simulations requiring large domains or complicated geometries.

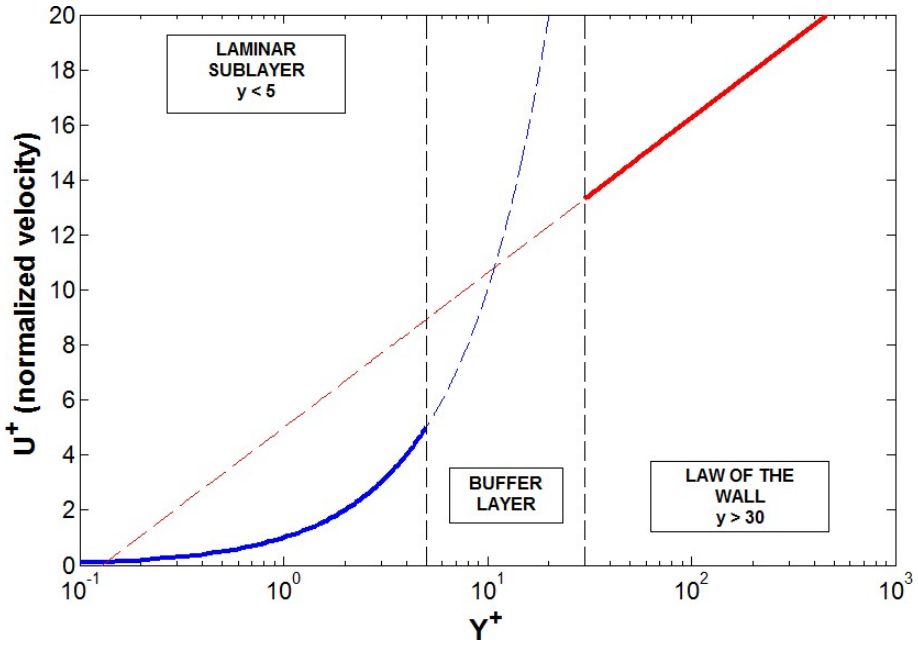

Figure 3.2: Near wall non-dimensional velocity profile

3.9 User Defined Functions (UDF)

A C or C++ function that may be dynamically loaded with the ANSYS Fluent 2023r1 solver to extend its built-in functionality is called a user-defined function, or UDF. A UDF can be used, for instance, to:

- Customize diffusivity functions, surface and volume reaction rates, material property definitions, boundary conditions and source terms in ANSYS Fluent 2023r1 transport equations.
- Modify calculated values once every loop.
- Set up a solution from scratch.
- Run at the conclusion of an iteration, when ANSYS Fluent 2023r1 is closed, or when a built UDF library loads.

3.9.1 Implementation of UDF

Function declarations provided by ANSYS Fluent 2023r1 are used to define UDFs. The UDF library contains these function declarations as DEFINE macros since they are implemented as macros in the code. The `udf.h` header file contains definitions for DEFINE macros and some of the macros are listed in Table 2.

DEFINE Macro	Function
DEFINE_ADJUST	Manipulates variables
DEFINE_EXECUTE_AT_END	Executes at end of iteration
DEFINE_INIT	Initializes variables
DEFINE_PROPERTY	Property customization
DEFINE_SPECIFIC_HEAT	Enthalpy and specific heat

Table 3.1: Macros in Fluent 2023r1

DEFINE_ADJUST macro: DEFINE_ADJUST is a general-purpose macro that can be used to adjust or modify ANSYS Fluent 2023r1 variables that are not passed as arguments. For instance, you can compute integrals and alter flow variables using DEFINE_ADJUST. Additionally, it can be used to integrate a scalar quantity throughout a domain and modify a boundary condition in response to the outcome. Before transport equations are solved, a function created with DEFINE_ADJUST is called at the start of each iteration and runs at every iteration.

DEFINE_EXECUTE_AT_END macro: A general-purpose macro called DEFINE_EXECUTE_AT_END is invoked at the conclusion of a time step in a transient run, or at the end of an iteration in a steady-state run. DEFINE_EXECUTE_AT_END can be utilized to compute flow quantities at these specific intervals.

DEFINE_INIT macro: DEFINE_INIT is a general-purpose macro that you can use to specify a set of initial values for your solution. By using DEFINE_INIT macro, it achieves the same goal as patching but in a different manner. The DEFINE_INIT function is run immediately after the solver completes its default initialization, and it is only executed once per initialization. It is usually

used to set initial values of flow quantities because it is called after the flow field is setup.

DEFINE_PROPERTY macro: DEFINE_PROPERTY is used to specify a custom material property in ANSYS Fluent 2023r1 for single phase and multiphase flows. Some of the properties that can be customized using DEFINE_PROPERTY are density, viscosity, thermal conductivity, rate of strain, etc.

DEFINE_SPECIFIC_HEAT macro: For fluid, solid, and mixed materials, temperature-dependent functions for specific heat and enthalpy can be defined using the DEFINE_SPECIFIC_HEAT macro. It is imperative that these functions are defined consistently. Specifically, the temperature integral of the specific heat function should be the enthalpy function.

3.9.2 Integration of UDFs

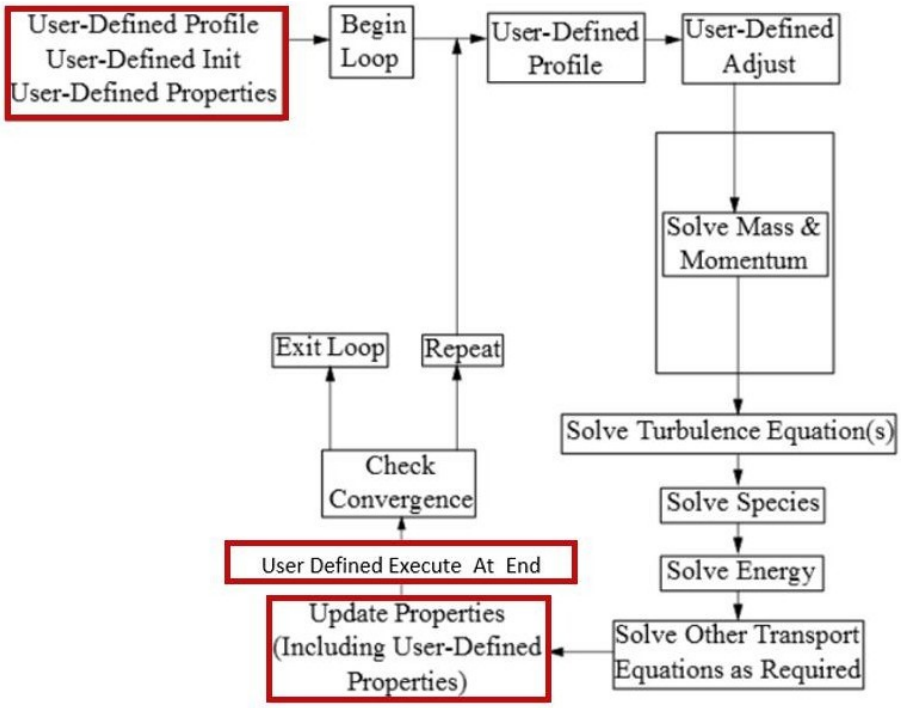

Figure 3.3: Solution Procedure in Fluent 2023r1 including UDF API calls

The solution procedure that is shown in Figure 3.3 is for a Pressure based Coupled solver. The highlighted blocks are the places where the used UDFs will get involved into the solving procedure which is important to know for the changing the material properties at the right time. The sequence begins by initializing equations to user-entered (or default) values taken from the ANSYS Fluent 2023r1 user interface. Next, PROFILE followed by INIT UDFs are called. Except the first iteration, PROFILE UDFs are executed prior to ADJUST UDFs. Then Fluent 2023r1 solves the mass and momentum equations followed by the turbulence and energy equation. After this, properties are updated, including PROPERTY UDFs. Therefore, given

the revised temperature and pressure, the density will be changed at this point if your model uses the gas law, for example. The loop either continues or ends after the convergence check has been made.

3.9.3 User Defined Memory (UDM)

User-defined memory locations that users can designate and use inside their UDFs are referred to as User Defined Memory (UDM) in Fluent 2023r1. In essence, UDMs are extra memory storage spaces that users can set aside and utilize in their UDFs to hold data that Fluent 2023r1 doesn't automatically supply. This enables users to add any custom data structures, arrays, or variables required for their unique simulation needs. When users need to track additional values or carry out unique computations that Fluent 2023r1's built-in functions don't support, UDMs come in handy. Users can increase the flexibility and capability of their Fluent 2023r1 simulations to suit their unique needs by creating and utilizing UDMs within their UDFs.

4

Model development

The main idea behind the tuned model is that will mimic the boiling process. The tuned model is developed by changing the fluid properties of the fluid that resembles boiling. The model once developed will be able to eliminate the need for a multiphase simulation and thereby greatly reducing the complexity of the problem as the need for resolving the secondary (gaseous) phase is eliminated. A number of important features of flow materials change significantly when water boils. As water heats up in the liquid phase, its density marginally reduces, but when it vaporizes into steam, it drastically lowers. Viscosity also decreases with temperature in the liquid phase and drastically reduces in the vapor phase. Heat transfer rates are impacted by the modest drop in thermal conductivity in the liquid phase and the considerable decrease in thermal conductivity in steam. Liquid water has a relatively high specific heat capacity, compared to the vapor phase and gradually drops with temperature once the fluid is in the vapor phase. For the boiling process to be effectively modeled, these changes in characteristics are necessary.

Another important aspect that needs to be modelled to get accurate results is the mixing of the phases which will have direct impact in the flow regimes in turn it plays a crucial role in heat transfer. The turbulent mixing might be important in both the pressure drop and heat transfer predictions. However, the starting flow property changes were done only for density, specific heat, viscosity and thermal conductivity were changed as these are the known changes that happens during boiling.

Then the next challenge is the method of implementation to mimic the boiling process. This is achieved with the help of UDFs in ANSYS Fluent. The material properties such as density, thermal conductivity and viscosity are changed from the liquid's to the vapor's in a linear fashion. Specific heat is varied as to compensate the enthalpy addition that is need for a phase change process.

4.1 Fluid Property Changes

4.1.1 Density Change

As water boils, its density decreases due to the phase transition from liquid to vapor. In the liquid phase, water molecules are closely packed, resulting in high density. When heated, the kinetic energy of the molecules increases, overcoming intermolecular forces and causing the transition to vapor. In the vapor phase, molecules are more dispersed, occupying a larger volume and resulting in significantly lower density compared to the liquid phase.

For the following simulations, the density of the fluid is changed with the help of vapor quality.
Vapor quality is defined as the proportion of the vapor phase that is in the fluid mixture relative to the total mixture and it is expressed as,

$$x = \frac{m_{\text{vapor}}}{m_{\text{total}}} \tag{4.1}$$

An alternative definition of vapor quality which can be used for single component mixtures like water and steam is,

$$x = \frac{h - h_l}{h_{lv}} \tag{4.2}$$

where

- h is the mixture enthalpy
- h_l is the saturation enthalpy of the liquid
- h_{lv} is the latent enthalpy

The above equation was used to create a User Defined Memory (UDM) in Fluent in order to track the vapor quality across the domain.

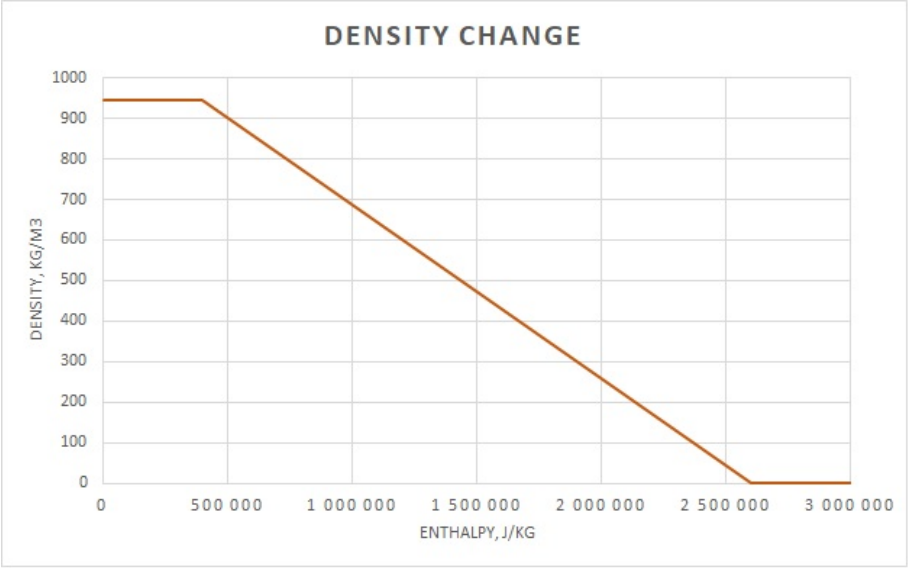

Figure 4.1: Density change

This created vapor quality variable which depends on the enthalpy is used to change from the density of the liquid to the density of steam during the boiling the phase which is shown in Figure 4.1.

4.1.2 Viscosity Change

When water boils, its viscosity decreases. Viscosity, the resistance to flow, is higher in liquid water due to strong intermolecular forces. As water heats, molecules gain kinetic energy, overcome these forces, and transition to the vapor phase. In the vapor phase, molecules are more dispersed and mobile, leading to significantly lower

viscosity compared to the liquid state. This phase shift reduces flow resistance and reflects the lower viscosity of water vapor. The same method which was used to change density during boiling is employed during boiling was used here as well. That is, vapor quality which is defined using the enthalpy and stored in an UDM is used to reduce viscosity during boiling and the viscosity change in shown in Figure 4.2.

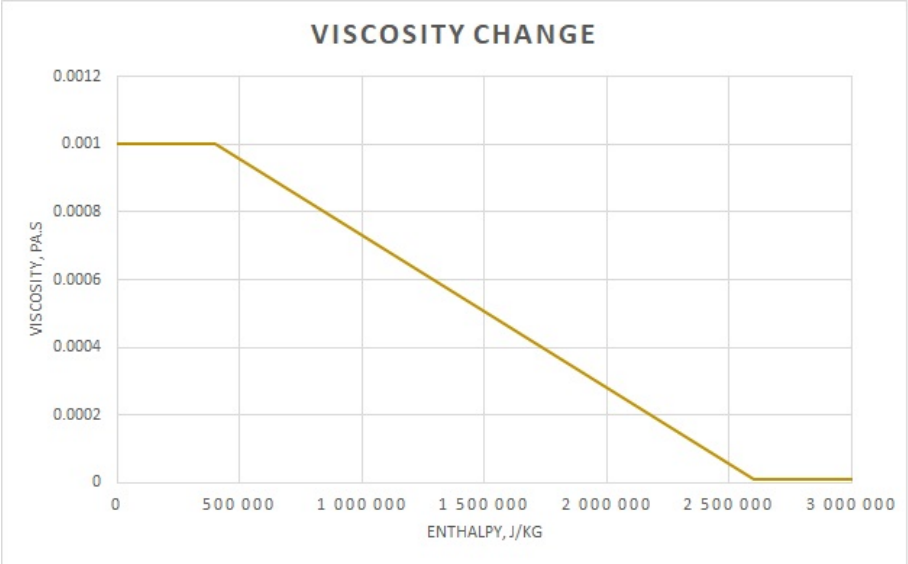

Figure 4.2: Viscosity change

4.1.3 Thermal conductivity Change

As discussed for the other two parameters, the thermal conductivity is changed in a similar fashion and the change is shown in Figure 4.3.

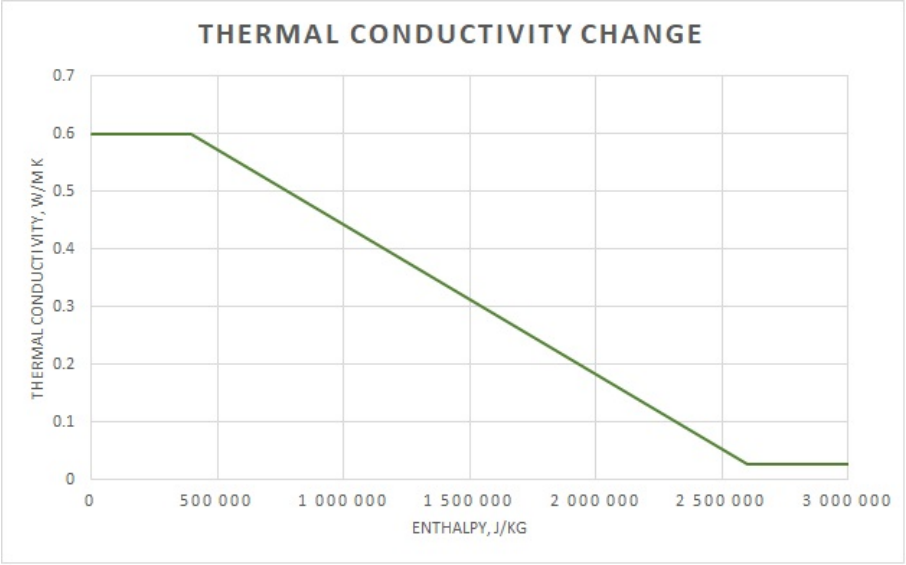

Figure 4.3: Thermal conductivity change

4.1.4 Specific heat Change

The modelling of specific heat is a bit challenging as boiling takes place at constant temperature and this in turn means that the specific heat while boiling turns into infinity. As that is impossible to model and as the boiling region is assumed to be 10K. The boiling region was fixed after simulating for different boiling regions between 2 and 12K and the smaller boiling regions were unstable for simulations and the range between 8 and 12K had a stable solution. The specific heat was modelled with the help of a hat function. A hat function is a function whose graph takes a triangular shape.

The magnitude of the hat function was determined by estimating the peak specific heat in the triangular function such that the area under the triangular function gives the latent enthalpy for the specific problem. The latent enthalpy should be equal to the area of the triangle and that is given by,

$$h_{lg} = \frac{\text{Height}(C_{p,\max}) \cdot \text{Breadth}(\Delta T)}{2} \tag{4.3}$$

where

- h_{lg} is the latent enthalpy
- $C_{p,\max}$ is the maximum magnitude of specific heat, which is the height of the triangle
- ΔT is the boiling region

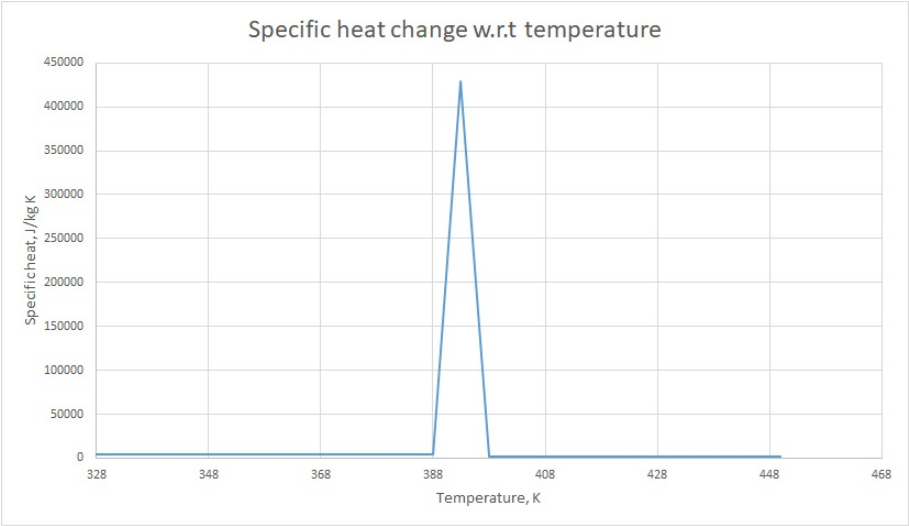

Figure 4.4: Specific heat change

In Figure 4.4 , the specific heat change is shown for the operating pressure of 200kPa. The saturation temperature of water at 200kPa is 393K. The latent enthalpy of water is 2201500 J/kg. From the equation above, the height i.e. the maximum specific heat was found to be 440300 J/kg K.

4.2 Sequence of property changes

After the property change methods are finalized, the important thing is the order of the change of the properties. The first property that is changed is the specific heat as that is an important parameter in having the correct amount of heat that is added into the system. As the specific heat is changed with respect to temperature, the enthalpy is also changed accordingly with respect to temperature to balance the heat addition. The 'Define specific heat' macro is used for the change which can be seen in Figure 15 is executed before the 'Execute at end' macro which is used to change the density based on enthalpy. Enthalpy is used as the changing parameter for density, thermal conductivity and viscosity so as to give some stability to the solver because when all the parameters are changed based on temperature, the system becomes highly unstable to solve.

5

Model Validation

The process of evaluating and verifying a method or procedure's accuracy, suitability, and reliability for its intended use is known as method validation. Validating a method assures that the procedures, models, or approaches employed may provide accurate and significant outcomes, which are critical for regulatory compliance, decision-making, quality control, and project success. After the successful development of the tuned model, it is essential to test and validate the accuracy of the tuned model. The validation of the tuned model is done against a research paper which has a working medium of water and the experiments done on horizontal pipe. The following section explains in detail about the experiment on which the tuned model is validated.

5.1 Experimental test case

The main focus of Yu et.al [21] for the experiments was to conducts tests on a short horizontal tube with an inside diameter of 2.98 mm and a heated length of 0.91 m was used to study the two-phase pressure drop, boiling heat transfer, and critical heat flux to water. The 200 kPa system pressure, 50–200 kg/m2s mass flux, and ambient to 80 °C input temperatures were all used during the experiments. Experimental findings and their comparison with prediction correlations were also done. The main driving force behind the selection of Yu paper is that first and foremost the working medium is water. The experiments are done in horizontal pipes which is important as well. The working conditions used for the experiments had a good range of interest for the heat exchanger of our interest as well. For these reasons, the tuned model is validated against the Yu paper and the experimental setup and the results are explained in the following section.

5.1.1 Experimental setup description

The experimental setup by Yu was fabricated in order to investigate two-phase pressure drop, boiling heat transfer, and CHF of flowing water, ethylene glycol, and aqueous mixes of ethylene glycol at high temperatures (up to 250°C) and low pressures (<345 kPa).

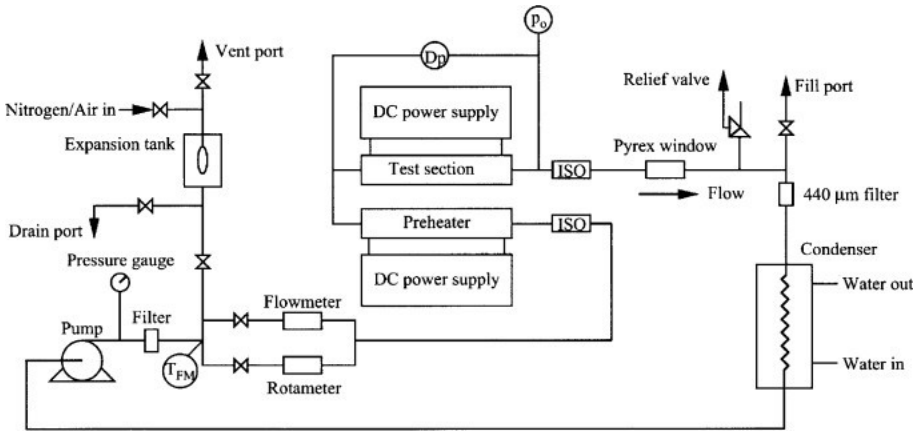

Figure 5.1: Experimental setup [21]

Figure 5.1 shows the experimental setup where the fluid is pumped via a loop and pressurized with an expansion tank. By changing the expansion tank's pressure, the test section's pressure can be regulated. To measure two ranges of volumetric flow rate, two flow measurement devices—a rotameter and a turbine-type flowmeter—are used in parallel configuration. The assessment of fluid density and, in turn, the computation of mass flow rate are made easier by the placement of a temperature sensor upstream from the flowmeters. An AC adjustable-frequency drive is used to fine-tune the flow rate. The fluid travels through a preheater system after the flowmeters, where it is heated to the appropriate subcooled level for that particular test. A Type 304 stainless steel tube of 500 mm in length, 4.57 mm in inner diameter, and 6.10 mm in outer diameter makes up the preheater. The preheater tube wall is subjected to resistance heating with the application of low-voltage direct current from a regulated power source. The power supply can produce up to 10 kW of power and provides accurate regulation within a range of 0.1% of the voltage or current.

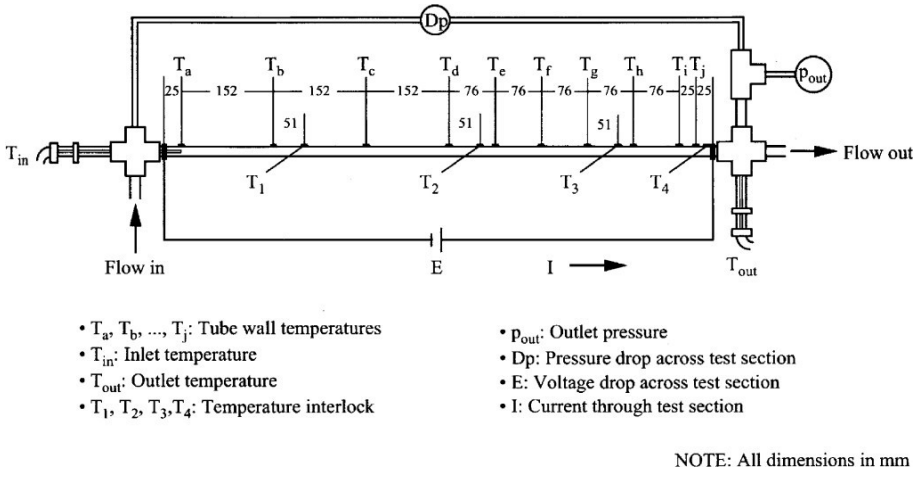

Figure 5.2: Experimental test section [21]

The fluid enters the experimental test portion, which is schematically depicted in Figure 5.2, after going through the preheater. The test section is heated using a separate power supply from the preheater. The current is calculated by measuring

the voltage drop across a shunt resistor, and the voltage drop across the test section is monitored directly. The product of the voltage drop and the current is used to determine the power (or heat) supplied to the test area. The flow pattern is visible through a Pyrex glass just beyond the experimental test area.

5.1.2 Yu experiment results

Yu had done tests with varying inlet temperature and varying mass fluxes to see the effect on wall superheat for different heat flux cases. Figure 5.3 is the results plot from Yu for constant mass flux and varying inlet temperature for different heat flux cases.

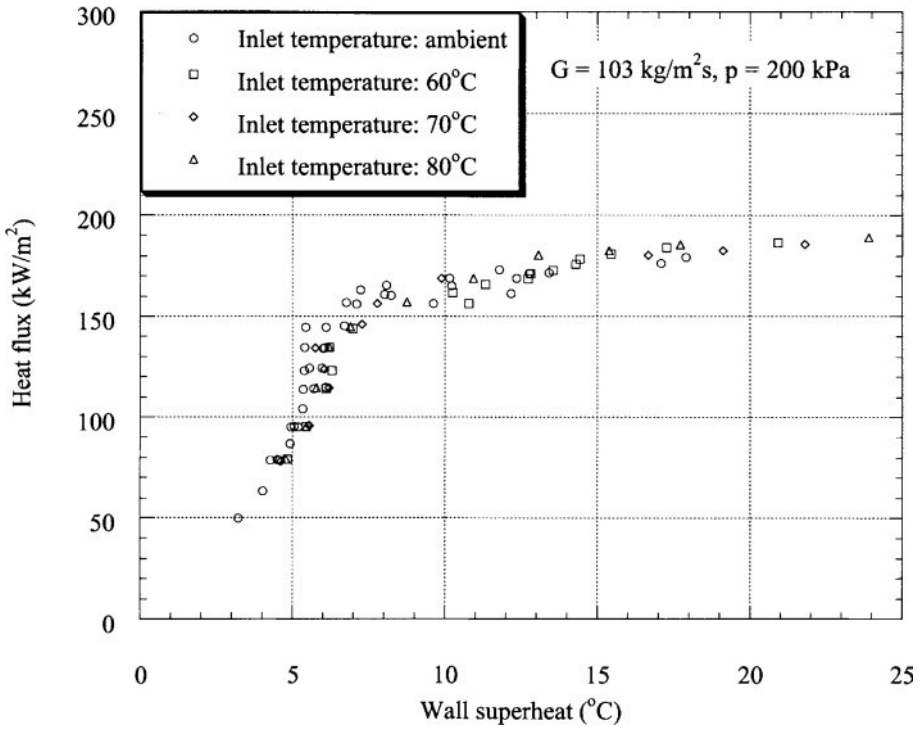

Figure 5.3: Experimental results [21]

5.2 Results

5.2.1 Single Phase Simulations

Before the multiphase approximations are done, it is important to verify if the problem setup and the mesh are generally reliable and can be trusted. To ensure this, a pipe geometry, shown in Figure 5.4, has been simulated with certain initial conditions and then compared with the single-phase correlations for estimating the pressure drop and heat transfer discussed in the previous chapter.

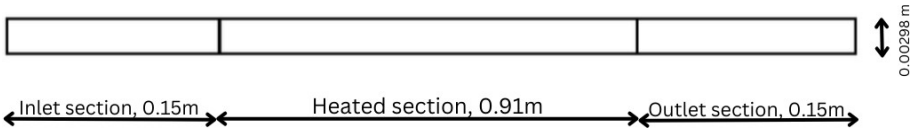

Figure 5.4: Single phase - geometry

5.2.1.1 Problem Description

The test section used for the simulation is shown in Figure 5.4. The test section is a circular pipe with a diameter of 0.00298 m. The heated section is 0.91 m, and there is an inlet section of 0.15 m (L/D = 50) for the flow to develop hydrodynamically and an outlet section of 0.15 m to avoid any instabilities in the simulations. The test section is the same as the experiments done by Yu et al.
A number of simulations were done at different Reynolds numbers ranging between 20,000 and 50,000. A constant heat flux of 100 kW/m^2 was applied to the heated section wall.

5.2.1.2 Mesh

A low Reynolds number mesh was used for all the simulations. A low Reynolds number mesh is preferred because it provides the necessary resolution to accurately capture the characteristics of the flows, resolve boundary layers, minimize numerical diffusion, ensure stability, and handle complex geometries effectively. This leads to more precise and reliable CFD simulations, which are essential for understanding and predicting the behavior of the flows.

Table 5.1: Mesh properties

Y+	2
Minimum cell height	$6{\cdot}10^{-6}$ m
Radial growth rate	1.2
Axial cell length	$1{\cdot}10^{-3}$ m
Axial growth rate	1

The mesh cell properties are shown in Table 5.1. A structured mesh was generated with the help of ANSA software. The mesh had 0.348 million cells. The cross-sectional view of the mesh is shown in Figure 5.5 and the front view of the mesh is displayed in Figure 5.6.

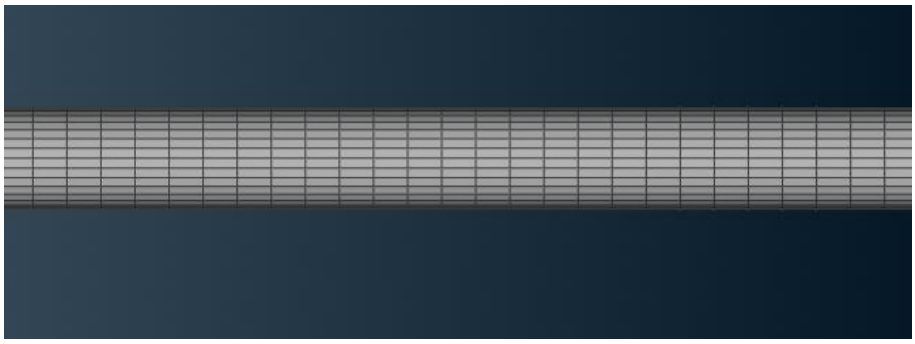

Figure 5.5: Cross-sectional view of the mesh

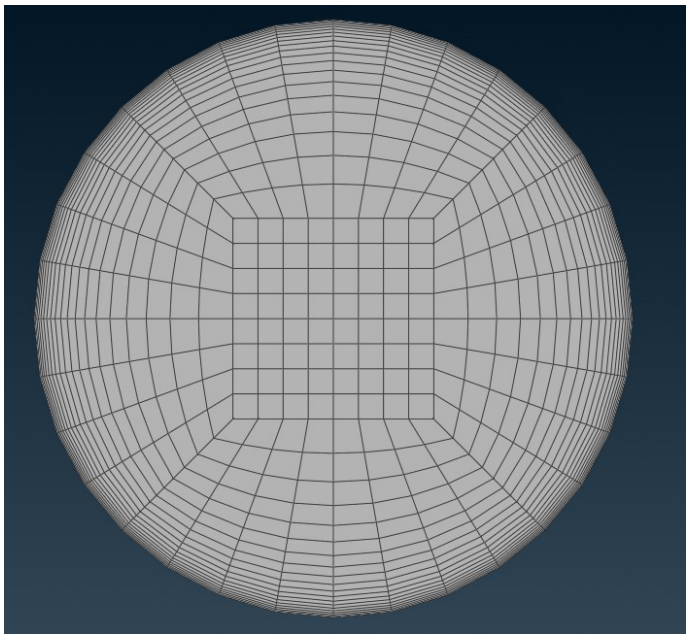

Figure 5.6: Front view of the mesh

5.2.1.3 Problem Setup

The working fluid used for the simulations is liquid water. The properties of water are set as variables with respect to temperature to achieve accurate results. The property changes with respect to temperature are inputted as a piecewise linear function in ANSYS Fluent 2023r1, as shown in Table 5.2.
After setting the temperature-dependent material properties, the simulations are run at atmospheric pressure. The inlet velocity is given as a velocity profile, shown in Figure 5.7, to ensure that the flow is completely developed at the entry of the heated section. The expression used is given below:

$$u(r) = u_{\max}\left[1 - \left(\frac{r}{R}\right)^{\frac{1}{4}}\right]^4 \tag{5.1}$$

Where:

- $u(r)$ is the velocity change in the radial direction
- $u_{\max}$ is the desired velocity

Table 5.2: Material property changes

Temperature (K)	Density (kg/m^3)	Specific Heat (kJ/kg · K)	Thermal Conductivity (W/m · K)	Viscosity (Pa · s)
298	997	4138	0.606	0.00089
333	983	3977	0.651	0.00046
353	972	3873	0.667	0.00035
373	958	3768	0.677	0.00028

- r is the inner diameter
- R is the outer diameter

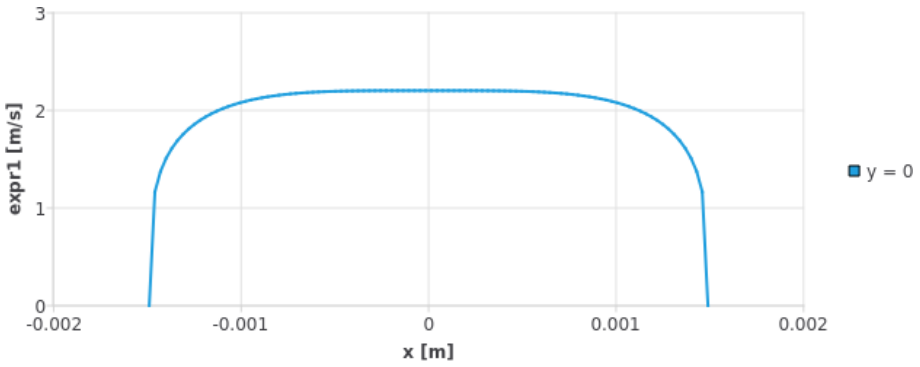

Figure 5.7: Inlet velocity profile

The solver settings used are as follows:

- **Pressure-Velocity Coupling**
  - Scheme: Coupled
- **Spatial Discretization**
  - Gradient: Least Squares Cell Based
  - Pressure: Second Order
  - Momentum: Second Order Upwind
  - Turbulent Kinetic Energy: Second Order Upwind
  - Specific Dissipation Rate: Second Order Upwind
  - Energy: Second Order Upwind
- **Turbulence Model**: k-ω SST model
- **Time Step Method**
  - Global time step with a Courant number of 200

5.2.1.4 Single phase results

5.2.1.4.1 Pressure Drop Comparison Figure 5.8 provides a clear comparison between the correlations and the simulation results. As shown, the simulation results agree well with the different correlations, with a maximum deviation of 2% when compared with the Moody correlation and a minimum deviation of 0.6% corresponding to the Blasius correlation.

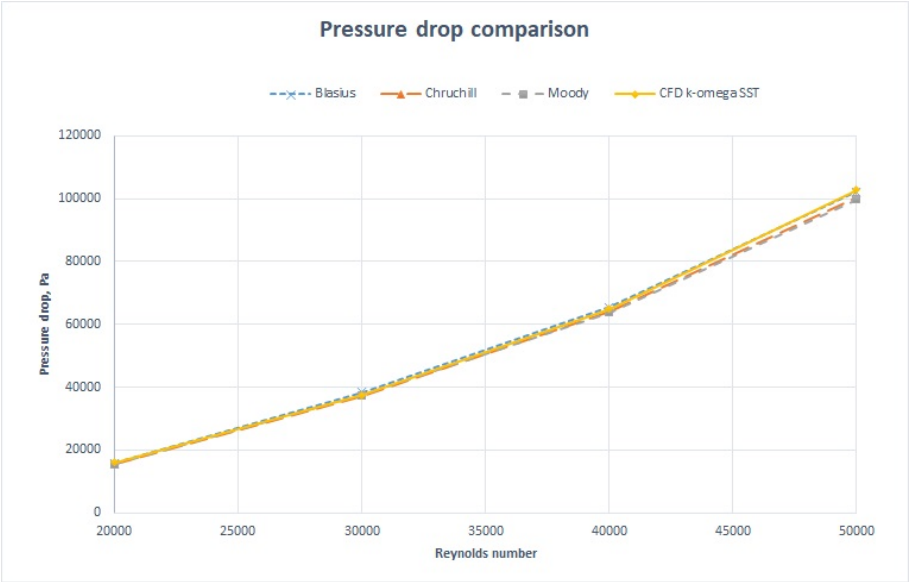

Figure 5.8: Pressure loss comparison

5.2.1.4.2 Heat Transfer Comparison Similar to the pressure drop comparison, the Nusselt numbers are also compared between the correlations and simulation results. Figure 5.9 shows that the Gnielinski correlation slightly overpredicts the Nusselt numbers against the simulation results, whereas the Sieder-Tate correlation underpredicts them. Nonetheless, the remaining correlations match quite well, with a minimum deviation found with the Dittus-Boelter correlation at 2.6% and a maximum with the Sieder-Tate correlation at 6%.

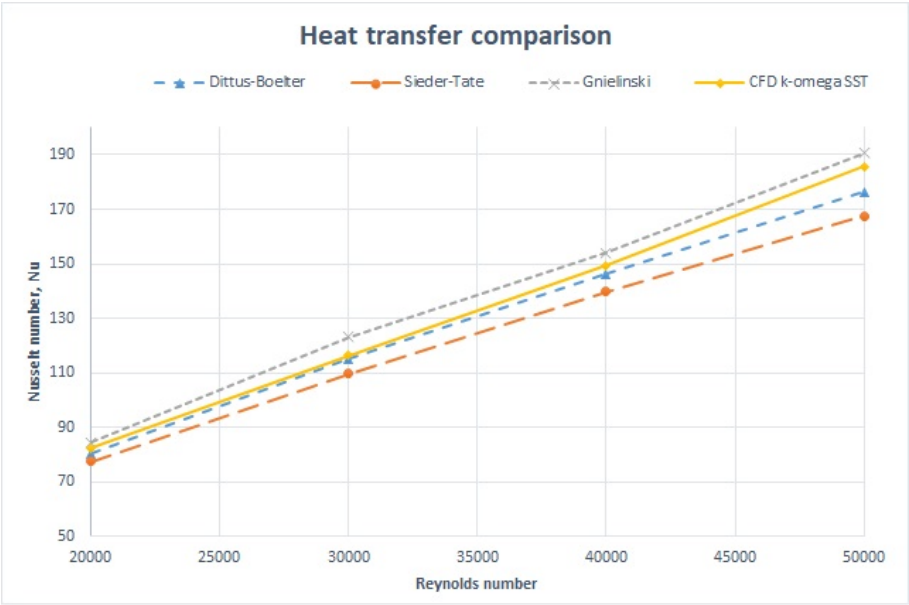

Figure 5.9: Heat transfer comparison

5.2.1.5 Summary

The main idea behind the single phase simulation and the comparison between the different pressure loss and heat transfer correlations was to validate the methodology for the simulation and then implement the learnings for the further simulations that were important.
From the pressure loss comparisons, it can be seen that the maximum deviation observed between the simulations and the correlations was just over 2%, which is an acceptable range. The minimum deviation was 0.6% when compared with the Blasius correlation, which is confirmed to be the best by Yu.
When the heat transfer correlations were compared with the simulation, the deviations observed were slightly higher compared to the pressure loss predictions. The maximum error observed between the simulation and the Sieder-Tate correlation was 6%, which is still a good prediction because the heat transfer correlations appear to be 20% off compared to the results obtained by Yu.

5.2.2 Multiphase Simulations

5.2.2.1 Problem Description

After completing the single-phase simulations, an overall picture of the simulation process is understood. The next step is to validate against the experimental data. The tests were conducted at a constant mass flux, and the operating pressure was the same throughout the different sets of experiments. In the simulations discussed in the following sections, the parameters in Table 5.3 were unchanged.

Table 5.3: Working conditions

Parameter	**Value**
Pressure	200 kPa
Mass flux	103 kg/m^{2}s
Inlet velocity	0.1092258 m/s
Mass flow rate	$6.57 \cdot 10^{-4}$ kg/s
Reynolds number	1300

The Reynolds number mentioned here is the Reynolds number at the inlet as the flow is entirely of liquid water.
Figure 5.3 shows the test results for constant mass flux and varying inlet temperature. However, for our study, four test points were taken, as shown in Table 5.4.

Table 5.4: Experimental test data points

Test case	**Heat flux (W/m^2)**	**Wall superheat (°C)**
1	80,000	5
2	115,000	6
3	160,000	9
4	180,000	13

From Table 5.4, Test Case 1 is selected as the base case for the initial assessment of the tuned model.

5.2.2.2 Mesh (Initial)

For the initial simulations to understand the CFD modeling methods, a low Reynolds number mesh is used. The front and radial views can be seen in Figure 5.10, and the mesh properties are tabulated in Table 5.5.

Table 5.5: Initial simulation mesh properties

Property	**Value**
y+	2
Minimum cell height	$5{\cdot}10^{-5}$ m
Radial growth rate	1.2
Axial cell length	$2{\cdot}10^{-3}$ m
Axial growth rate	1

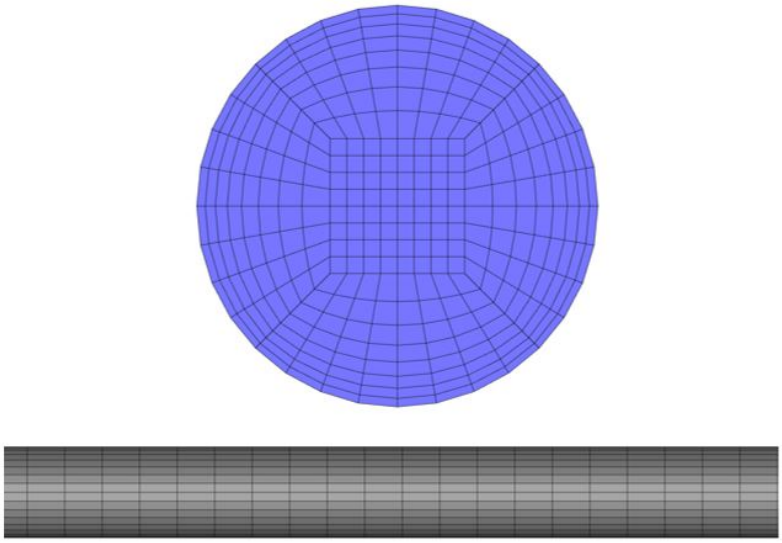

Figure 5.10: Initial simulation mesh: (a) Front view, (b) Radial view

5.2.2.3 Problem Setup

5.2.2.3.1 CFD Modelling Strategy Steady-state simulations were performed on a 3-D geometry of the horizontal tubes using the Fluent 2023r1 solver in double precision. Single-phase simulations were performed using the tuned fluid with property changes described in the previous section. A velocity inlet boundary condition was applied to the inlet, and a pressure outlet boundary condition was set at the outlet. A constant wall heat flux was applied to the tube walls. The solver settings used were almost identical to those in the single-phase simulations, except for changes in relaxation factors and the time step method.
The solver settings were as follows:

- **Pressure-Velocity Coupling**
  - *Scheme*: Coupled

- **Spatial Discretization**
  - *Gradient*: Least Squares Cell-Based
  - *Pressure*: Second Order
  - *Momentum*: Second Order Upwind
  - *Turbulent Kinetic Energy*: Second Order Upwind
  - *Specific Dissipation Rate*: Second Order Upwind
  - *Energy*: Second Order Upwind
- **Turbulence Model**
  - SST $k-\omega$: The single-phase simulations showed that this turbulence model performed well for both pressure drop and heat transfer prediction.
- **Relaxation Factors**

The relaxation factors used in the simulation are shown in Table 5.6.

Table 5.6: Relaxation factors

Pressure	Momentum	Density	Body Forces	Turbulent Kinetic Energy (k)	Specific Dissipation Rate (ω)	Turbulent Viscosity	Energy
0.5	0.5	0.2	1	0.75	0.75	1	0.3

- **Time Step Method**
  - Pseudo Time Method is used with a time scale factor of 0.4 to ensure stability while solving. The time scale factor was chosen after a series of simulations where the simulation was unstable with a time scale factor greater than 0.4.

5.2.2.3.2 Convergence The simulation is considered to be converged when the residuals and monitor plots have reached a constant value. The residual plot is shown in Figure 5.11.

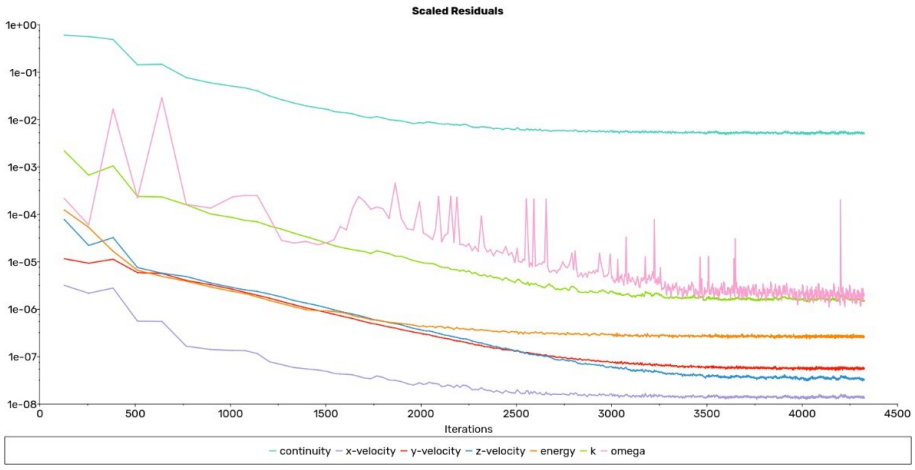

Figure 5.11: Convergence check – residuals

The monitor plots shown in Figure 5.12 and Figure 5.13 were used to check for convergence, displaying the area-averaged temperature at the walls and the area-averaged vapor quality (defined using a UDM) at the outlet.

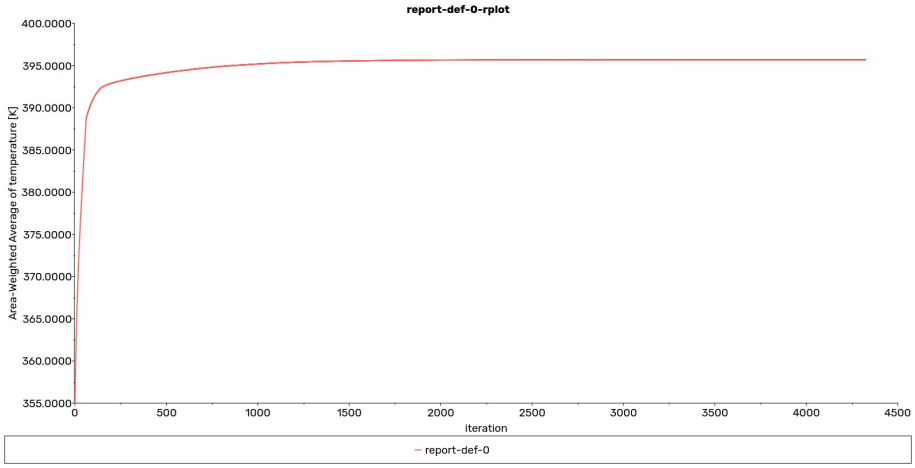

Figure 5.12: Area averaged wall temperature report

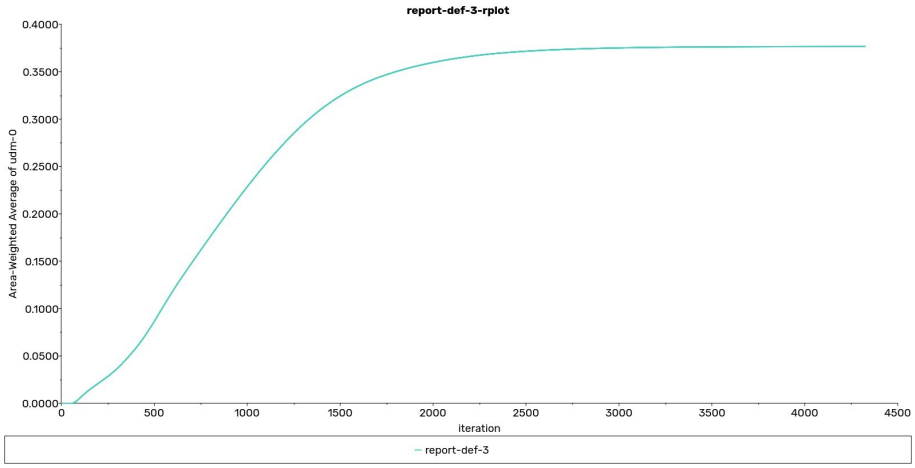

Figure 5.13: Area weighted average of vapor quality at outlet

After the learnings from the single-phase simulations, the tuned model was tested against the chosen experimental data by Yu, as explained in Section 5.1.

5.2.2.4 Results

5.2.2.4.1 Two Property Change Simulations For the initial simulation, only two properties were changed during the boiling process: density and specific heat. These parameters were chosen to reduce complexity initially, thereby providing better stability and understanding of the model. Test case 1, set as the base case, was simulated with UDFs to change both parameters.
To assess the parameter changes within the bulk fluid, a line was created along the axial flow direction at the center of the pipe to observe temperature and vapor quality changes.
Figure 5.14 shows the temperature plot at the center of the pipe along the flow direction. Ideally, the temperature of the fluid should remain constant during boiling. However, the plot indicates that the temperature does not stay constant during boiling, indicating inaccuracies in mimicking the boiling process.

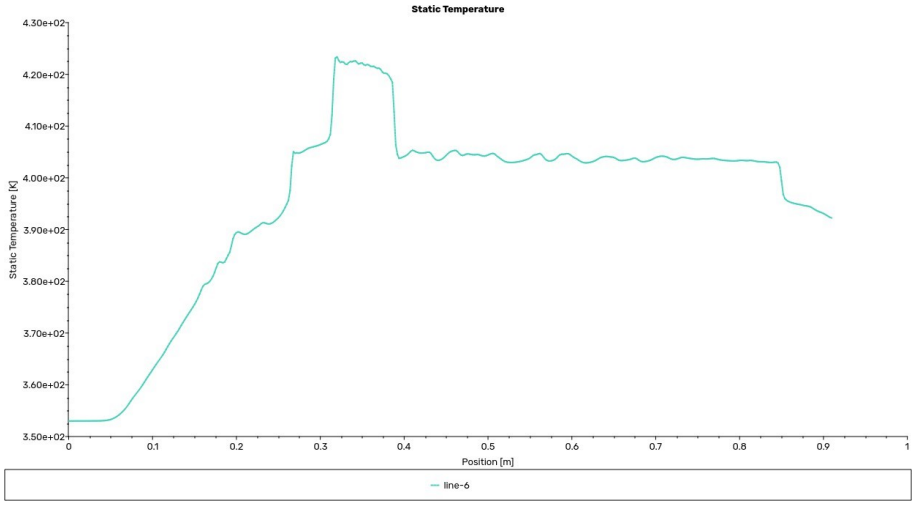

Figure 5.14: Static temperature - two property change

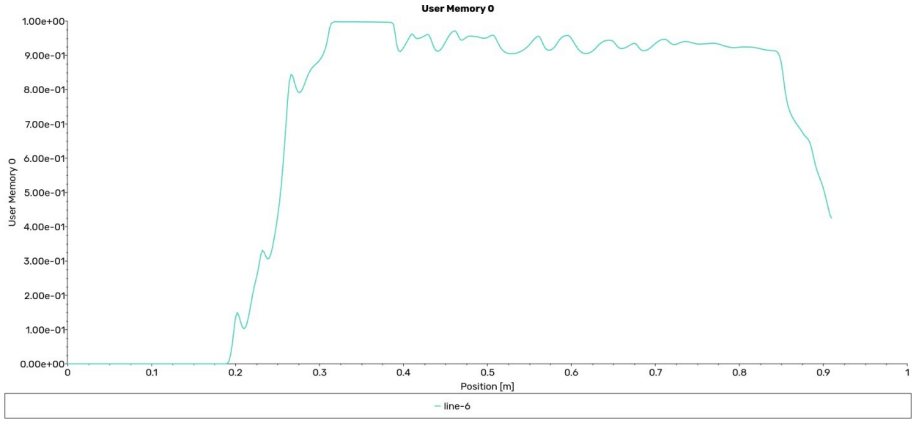

Figure 5.15: Vapor quality - two property change

Figure 5.15 displays the vapor quality plot along the flow direction at the center of the tube. The vapor quality should ideally rise from 0 to 1 during boiling and then remain constant. However, the plot shows instability and a sudden drop near the outlet, indicating an inaccurate simulation of the boiling process.
From these results, it is evident that the simulations do not accurately mimic the boiling process, as the enthalpy at the outlet is higher than expected based on the heat balance equation, leading to over-predicted vapor quality at the outlet.

5.2.2.4.2 Four Property Change Simulations From the learnings in Section 5.2.2.4, it is understood that changing only density and specific heat is not sufficient to accurately replicate the boiling process. To better mimic the boiling process, all four material properties—density, specific heat, thermal conductivity, and viscosity—were changed as discussed in Section 4.1.
Figure 5.16 shows the temperature change along the flow direction at the center of the tube. It is evident that the change in temperature along the tube is much more stable compared to the two property change simulations. The temperature change appears more physical: it rises rapidly until it reaches the start of the boiling region,

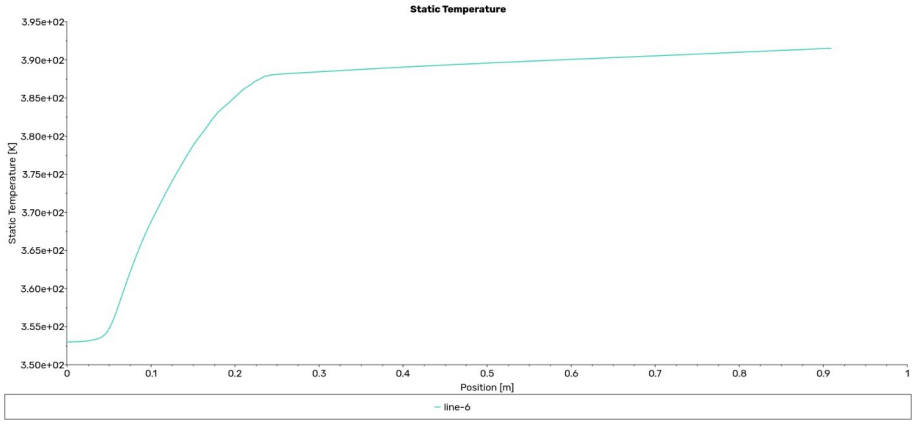

Figure 5.16: Static temperature - four property change

after which the temperature remains constant or stays within the boiling region.

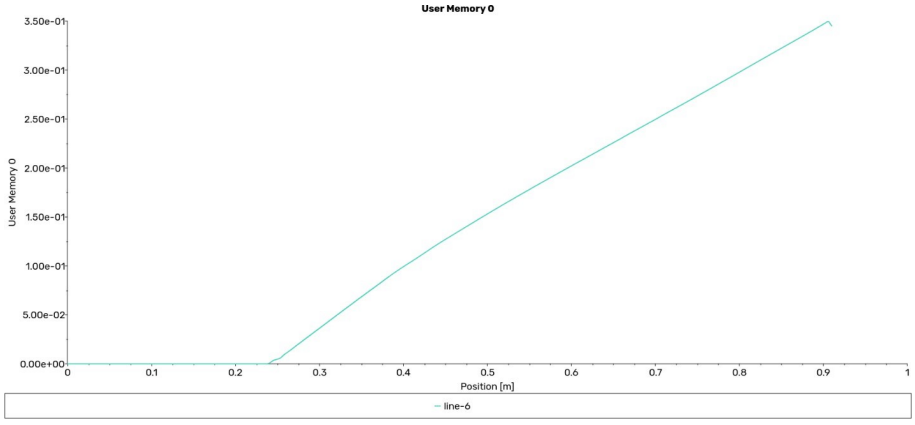

Figure 5.17: Vapor quality - four property change

Figure 5.17 shows the vapor quality change along the flow direction at the center of the tube. When comparing Figures 5.16 and 5.17, it can be seen that when the temperature reaches the start of the boiling region, the vapor quality starts to increase. The vapor quality continues to increase until the outlet as the temperature remains within the boiling region. This behavior demonstrates clear physical characteristics and effectively mimics the boiling process.
The changes in all four properties resulted in a much more accurate representation of the boiling process, as indicated by the stable temperature and increasing vapor quality profiles. This indicates that the tuned model with four property changes can effectively simulate the boiling process in a horizontal tube.

5.2.2.4.3 Influence of Mesh on Wall Temperature (Linearly Varying and Constant Thermal Conductivity) After finalizing the properties that need to be changed, the next step is to perform a mesh study to ensure the precision and reliability of computational outcomes. A mesh independence test is an essential stage in numerical simulations. The sensitivity of the solution to mesh refinement is evaluated by gradually changing the mesh density. This analysis accomplishes

multiple goals: it aids in estimating discretization error, provides information on the simulation's numerical accuracy, assesses convergence behavior to see if the solution stabilizes as mesh density increases, and optimizes computing resources by determining the lowest mesh resolution required for acceptable accuracy. Ultimately, a successful mesh independence test increases confidence in the predictive power of computational models and confirms their relevance to real scientific and engineering problems.
A mesh independence study was conducted using a design from the Yu experiment. The simulation was performed with material property changes for density, viscosity, thermal conductivity, and specific heat. Simulations were conducted for different y+ meshes varying between y+ 2 and y+ 0.05, with the mesh refinement between two different mesh cases shown in Figure 5.18.

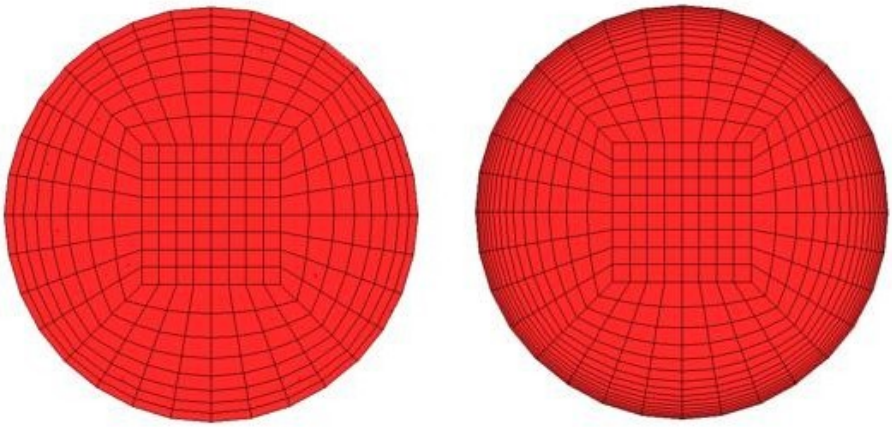

Figure 5.18: Mesh comparison

5.2.2.4.3.1 Mesh Study with Linearly Varying Thermal Conductivity
The linearly varying thermal conductivity case involves the simulation with the four parameter changes discussed in Section 4.1. For the mesh study, Test Case 1 is used as mentioned in Table 6, with a constant wall heat flux of 80,000 W/m^2. This case is set as the base case for our simulations, and the model is evaluated accordingly.

Table 5.7: Mesh study results – Linearly varying thermal conductivity

y+	Cell count	Wall temperature at the outlet (K)	Bulk temperature at the outlet (K)	Vapor quality
2	140,000	393.38	391.58	0.358
1	190,000	420.6	391.59	0.358
0.5	250,000	455.363	391.59	0.357
0.05	870,000	496.48	392.107	0.410

The wall temperature at the outlet is obtained from ANSYS Fluent 2023r1 by creating an iso-surface along the circumference at the pipe outlet. From Table 5.7, the wall temperature at the outlet can be seen to rise rapidly. On the other hand, the bulk temperature at the outlet, obtained by mass flow averaging the temperature

at the outlet, remains fairly constant, and the mass flow averaged vapor quality at the outlet is constant as well, except for the finest mesh.
To understand the increase in the outlet wall temperature, a graph is plotted in Figure 5.19 to analyze the outlet wall temperature for the corresponding wall y+. The dotted line in the figure represents the wall temperature at the outlet observed in the experiment performed by Yu et al. The outlet wall temperature was obtained from the wall superheat for the corresponding wall heat flux.

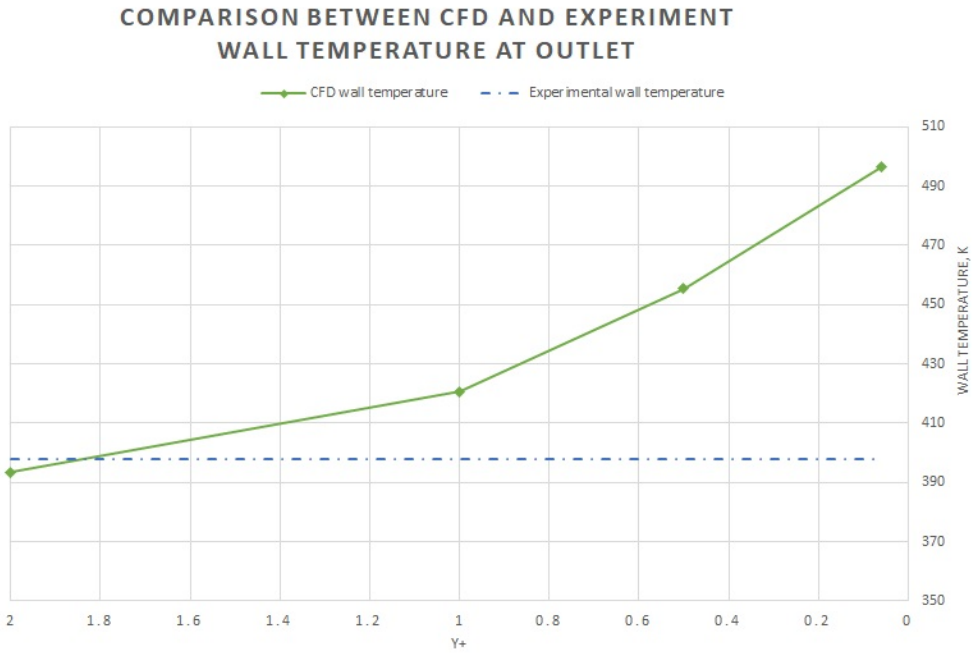

Figure 5.19: Wall temperature at the outlet vs. wall y+

From the plot, it could be seen that the increase in outlet wall temperature grows as the wall mesh refinement increases.

5.2.2.4.3.2 Results The heat transfer coefficient (HTC) is plotted in Figure 5.20 for the different heat fluxes simulated from Table 5.4. The experimental HTC was compared with the CFD results as well as the heat transfer correlations discussed in Section 2.7.2. According to Yu et al., the correlations were about 30% off the experimental results. However, the CFD results showed a very low HTC prediction. The main reason for this underprediction was the high wall temperatures observed earlier.
The difference between the experimental value and the outlet wall temperature is small only for a coarser mesh, which is still a low Reynolds number mesh. To better understand the cause of this high wall temperature, it is important to know how the constant wall heat flux is applied to the fluid. The heat flux entering the system, as defined in ANSYS Fluent 2023r1, is given by:

$$q = k_{\text{eff}} \frac{\partial T}{\partial y} \tag{5.2}$$

where:

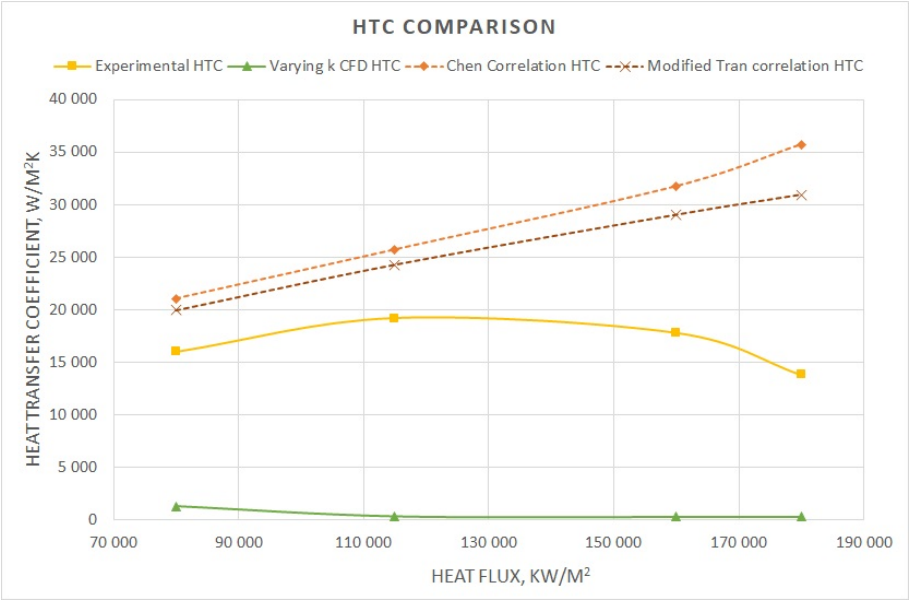

Figure 5.20: HTC comparison – Linearly varying k simulation

- q is the heat flux,
- k_{eff} is the effective thermal conductivity, which is the sum of molecular thermal conductivity and turbulent thermal conductivity, i.e.,
- $k_{\text{eff}} = k + k_t$
- $\frac{\partial T}{\partial y}$ is the temperature gradient normal to the wall.

To better understand the influence of effective thermal conductivity, the effective thermal conductivity is plotted radially at an axial location of about 90% from the inlet. Figure 5.21 illustrates the location at which the radial distribution of the effective thermal conductivity is plotted.

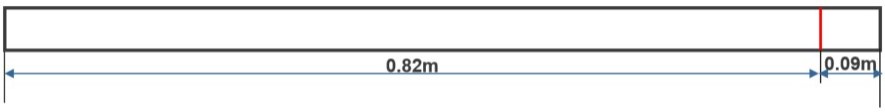

Figure 5.21: Axial location of analysis

The legends in the plots, where the coarse mesh represents the y+ 2 mesh and the fine mesh represents the y+ 0.4 mesh, are shown in Figure 5.22. The plots clearly show that the effective thermal conductivity is lower for a finer mesh compared to the coarse mesh.

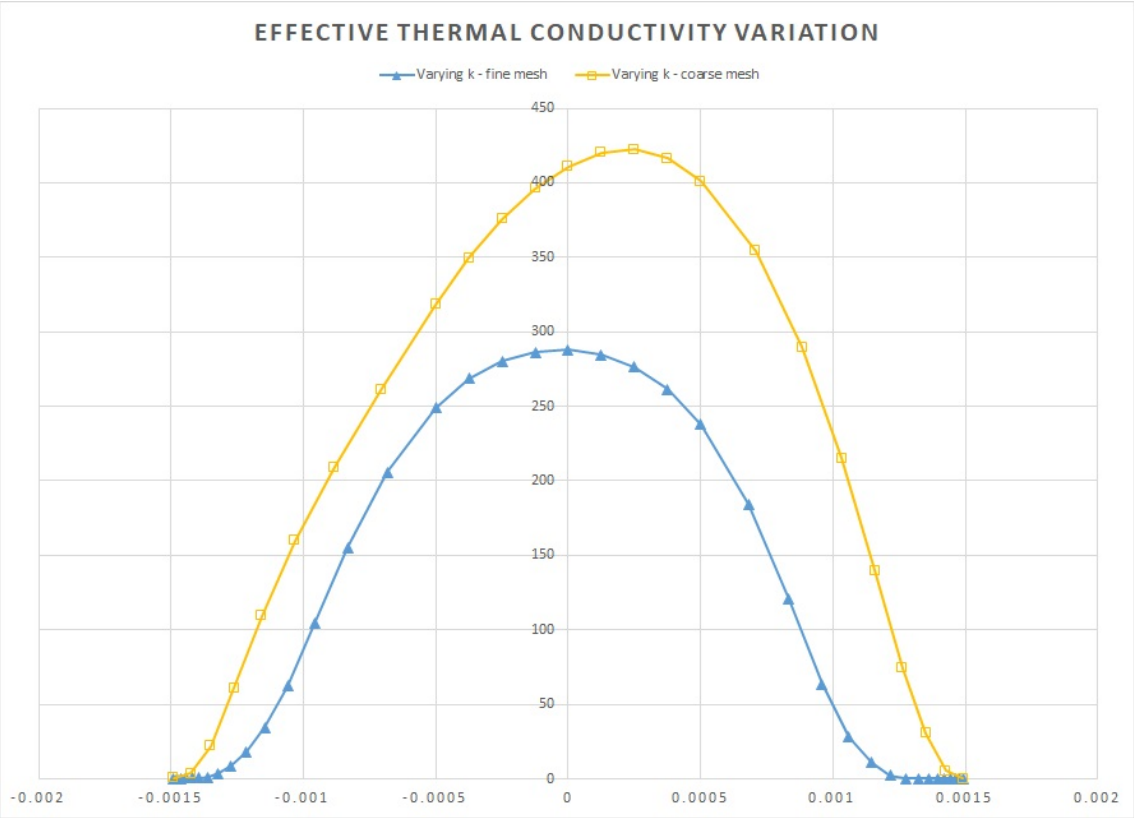

Figure 5.22: Effective thermal conductivity variation

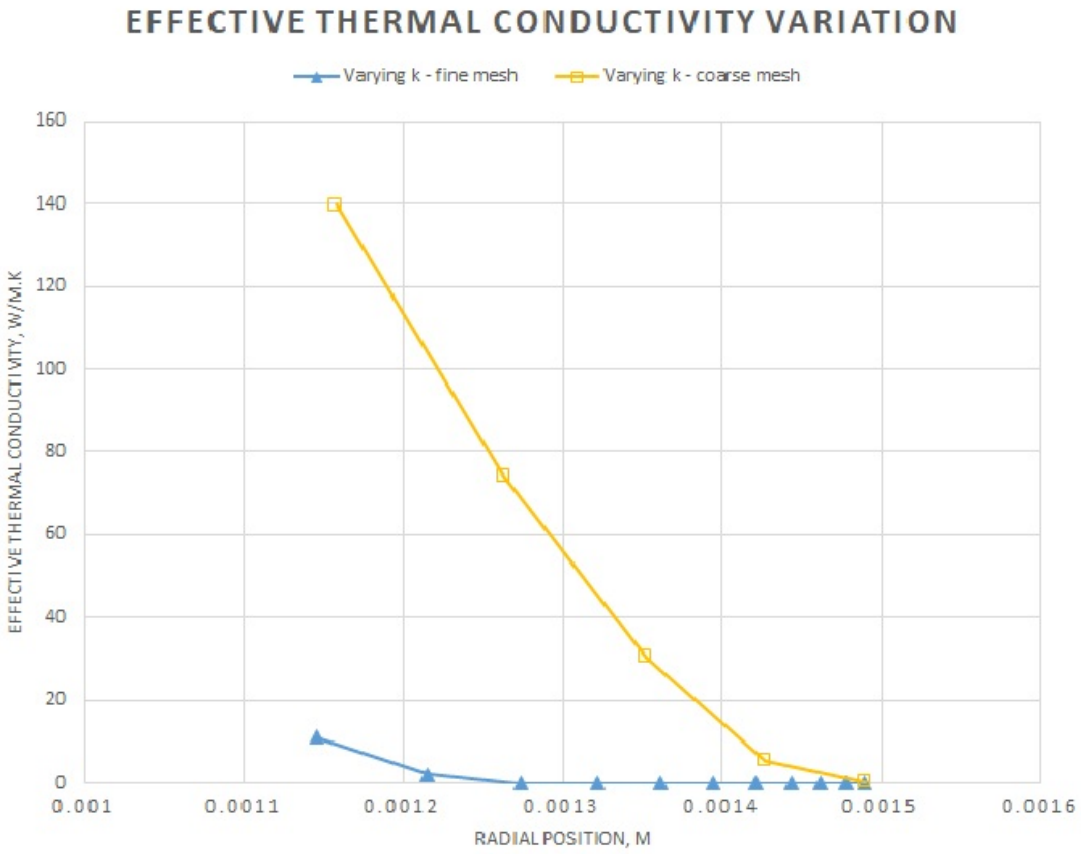

Figure 5.23: Effective thermal conductivity at the top wall

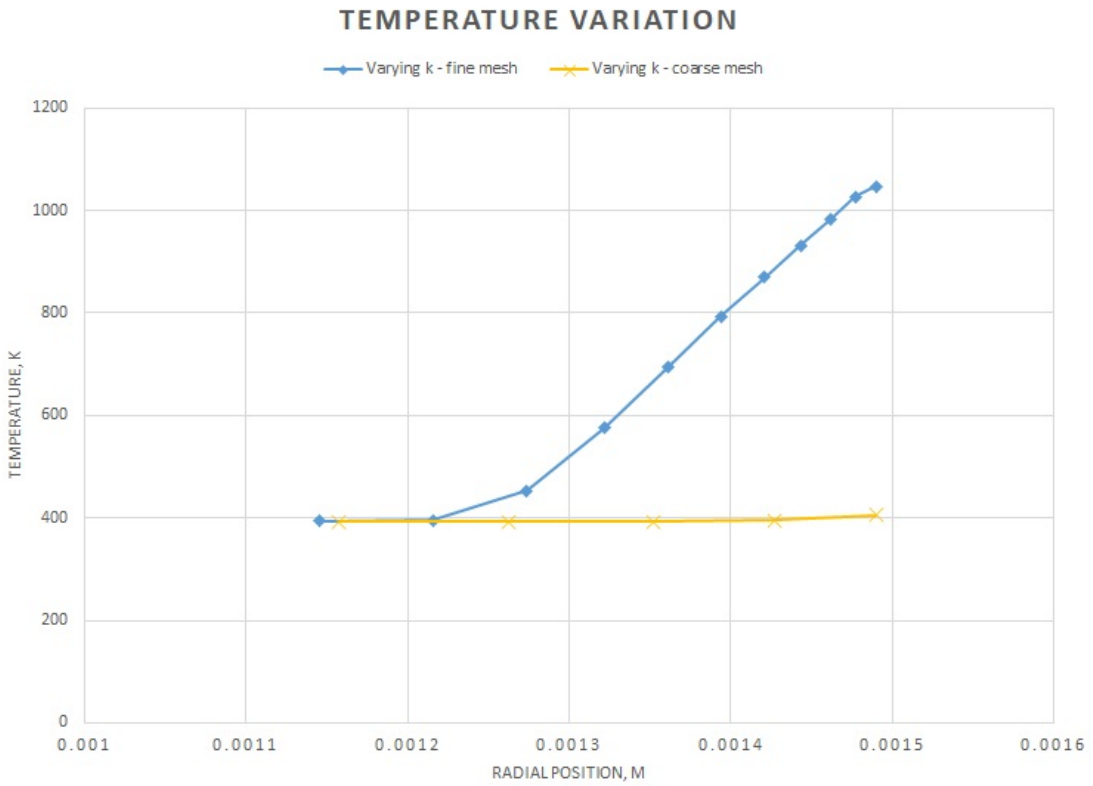

Figure 5.24: Temperature variation - top wall

The main discrepancy in the mesh independence study was the outlet wall temperature. To understand this better, Figure 5.23 shows a zoomed-in view of the values at the top wall. It is observed that the molecular thermal conductivity is dominant for a longer wall normal distance for the fine mesh compared to the coarse mesh. To analyze the influence of this molecular thermal conductivity dominance on the wall temperature, a similar plot to Figure 5.23 is plotted for temperature. It is clearly seen in Figure 5.24 that the wall temperature starts to rise as the turbulent thermal conductivity has less influence. From this analysis, it is understood that the wall temperature is highly dependent on the effective thermal conductivity, which is predominantly molecular thermal conductivity near the walls for a finer mesh due to the a bsence of turbulence near the wall. Moreover, the effective thermal conductivity is very sensitive to wall mesh refinement, even when using low Reynolds number meshes.

5.2.2.4.4 Mesh Study with Constant Thermal Conductivity To better examine the effect of thermal conductivity on the wall temperature for finer meshes, the same set of meshes were simulated for the base case as in the varying thermal conductivity cases. In this scenario, the fluid properties are varied as discussed in Section 4.1, except the molecular thermal conductivity, which is kept constant to that of the liquid. Table 5.8 provides the results for the mesh study performed with a constant thermal conductivity, while other properties such as density, specific heat, and viscosity were varied similarly to the previous simulations.

Table 5.8: Mesh study results - constant thermal conductivity

y+	Cell count	Wall temperature at the outlet (K)	Bulk temperature at the outlet (K)	Vapor quality
2	140,000	393.29	391.57	0.358
1	190,000	395.16	391.57	0.358
0.5	250,000	396.72	391.58	0.357
0.05	870,000	397.3	391.59	0.357

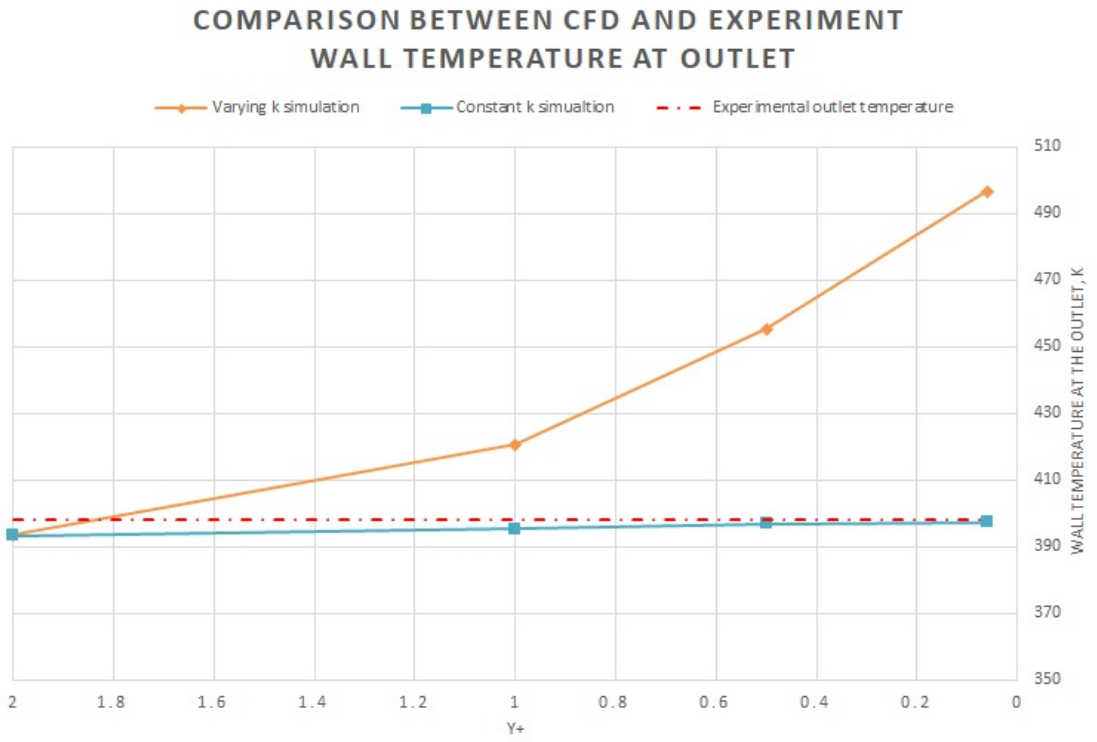

Figure 5.25: Wall temperature at outlet - constant thermal conductivity

Figure 5.25 shows the outlet wall temperature against the different meshes for both the varying thermal conductivity and constant thermal conductivity simulation cases, compared against the experimental outlet wall temperature for the specific test case. Comparing Table 5.8 and Table 5.7, it is seen that the bulk temperature at the outlet is the same for both varying thermal conductivity and constant thermal conductivity cases, whereas the outlet wall temperature is significantly influenced by the thermal conductivity. The constant thermal conductivity simulations show better agreement with the experimental outlet temperature.

5.2.2.4.4.1 Results Figure 5.26 gives the heat transfer coefficient compared with the experimental results and the correlations as it was done for the varying k simulation as well. The difference here is that the CFD simulations' HTC prediction is far more acceptable than when compared with CFD results from varying

thermal conductivity simulations. The maximum deviation that was found was 25%, which is still less than the average deviation found in the correlations.

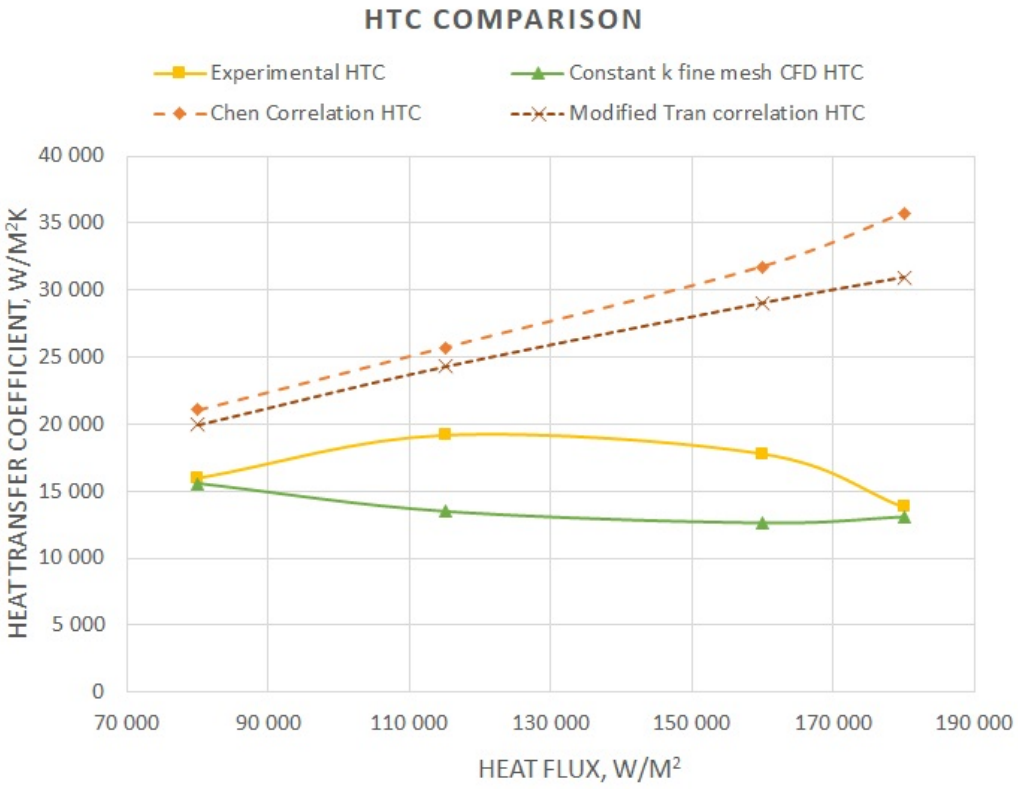

Figure 5.26: HTC comparison - constant k simulation

5.2.2.4.5 Comparison between Linearly Varying and Constant Thermal Conductivity As the reasoning behind the extremely high wall temperatures is highly dependent on the thermal conductivity change, it is essential to understand the differences between the varying thermal conductivity simulations and the constant thermal conductivity simulations which give reasonable results.

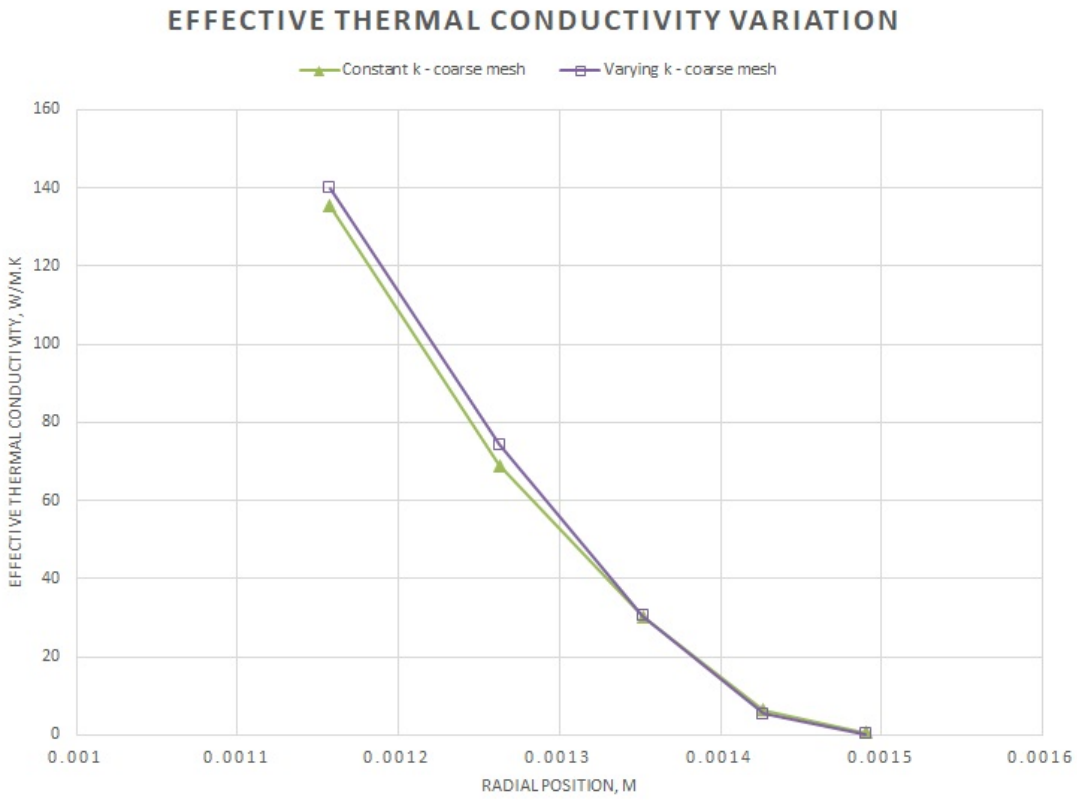

Figure 5.27: Effective thermal conductivity - coarse mesh

Figure 5.27 shows the effective thermal conductivity variation for the coarse mesh (i.e., $y^+ = 2$) and it is plotted at the top wall as it is the location where the temperature shoots up at an axial location of 0.82 m from the inlet, which is shown in Figure 40. It is observed that the two simulations are in great agreement with effective thermal conductivity at the top wall. This is reflected in the outlet wall temperature as well, as it can be seen in Figure 44 that the outlet wall temperature is the same for both the simulations.

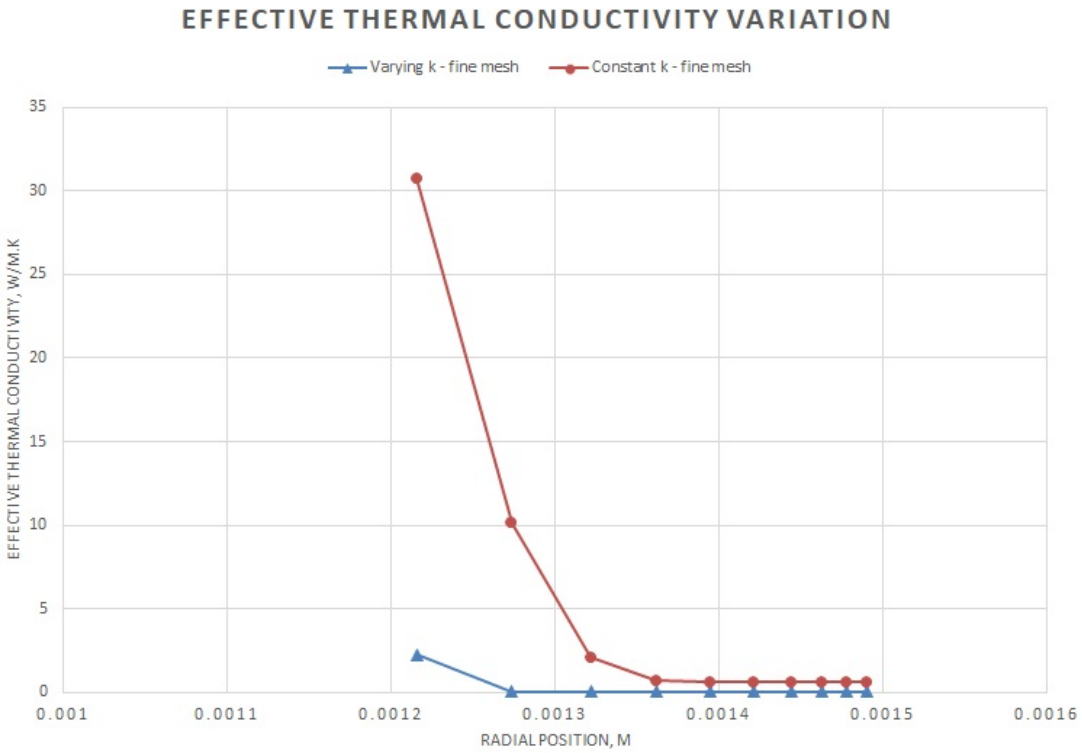

Figure 5.28: Effective thermal conductivity - fine mesh

Whereas from Figure 5.28, it is not the same case as the coarse mesh one, as there is a huge difference between the constant thermal conductivity simulation and varying thermal conductivity simulation for the fine mesh (i.e., $y^+ = 0.4$). The effective thermal conductivity for the varying case can be seen to be significantly less when compared to the constant thermal conductivity case. This is the reasoning behind the high wall temperature for the varying case as the effective thermal conductivity is low, the heat transfer efficiency drops accordingly.

5.2.2.4.6 Influence of Mesh on Wall Temperature (Blended k) After studying the influence of thermal conductivity, a blended function was used in modeling the thermal conductivity. This function is implemented to compensate for the lack of mixing of the two phases near the walls, which is the main issue for the increased wall temperature. The blended function is implemented from the start of the boiling region as,

$$k = C_k(x \cdot k_g + (1 - x) \cdot k_l) \tag{5.3}$$

Where

- k is the local thermal conductivity
- x is the local vapor quality
- k_g is the thermal conductivity of steam
- k_l is the thermal conductivity of water
- C_k is the tuning coefficient

The selection of the tuning coefficient is a trial and error process to determine which best matches the experimental results, which is a common approach in multiphase simulation solvers. The tuning coefficient compensates for the artificial addition of the turbulent mixing between the phases that occurs in single-phase simulation causing the wall temperature to increase.

5.2.2.4.7 Mesh Study with Blended Thermal Conductivity From the learnings that the modeling of thermal conductivity is crucial for accurate results, a tuning coefficient is introduced into the thermal conductivity UDF to improve the heat transfer efficiency near the walls, as it should increase for a phase change process like boiling. This is detailed in Appendix E – Blended Function Thermal Conductivity UDF. During and after boiling, a coefficient is multiplied by the thermal conductivity defined earlier using the linear function. The same meshes used for linearly varying and constant thermal conductivity simulations are used, and for this simulation, test case 2 from Table 5.4 was used. The results from the mesh study are shown in Table 5.9.

Table 5.9: Mesh study results - blended k

y+	Cell count	Wall temperature at the outlet (K)	Bulk temperature at the outlet (K)	Vapor quality
2	140000	394.82	393.43	0.543
1	190000	398.86	393.43	0.543
0.5	250000	399.64	393.44	0.543
0.05	870000	399.57	393.44	0.544

From Figure 5.29, it can be observed that the outlet wall temperature becomes stable as the mesh gets finer, and the coarsest mesh has a very low wall temperature. Thus, the blended method is stable and repeatable for meshes with y^+ less than 1. The experimental outlet temperature for the test case used for the simulation is also plotted, showing great agreement with the CFD results.

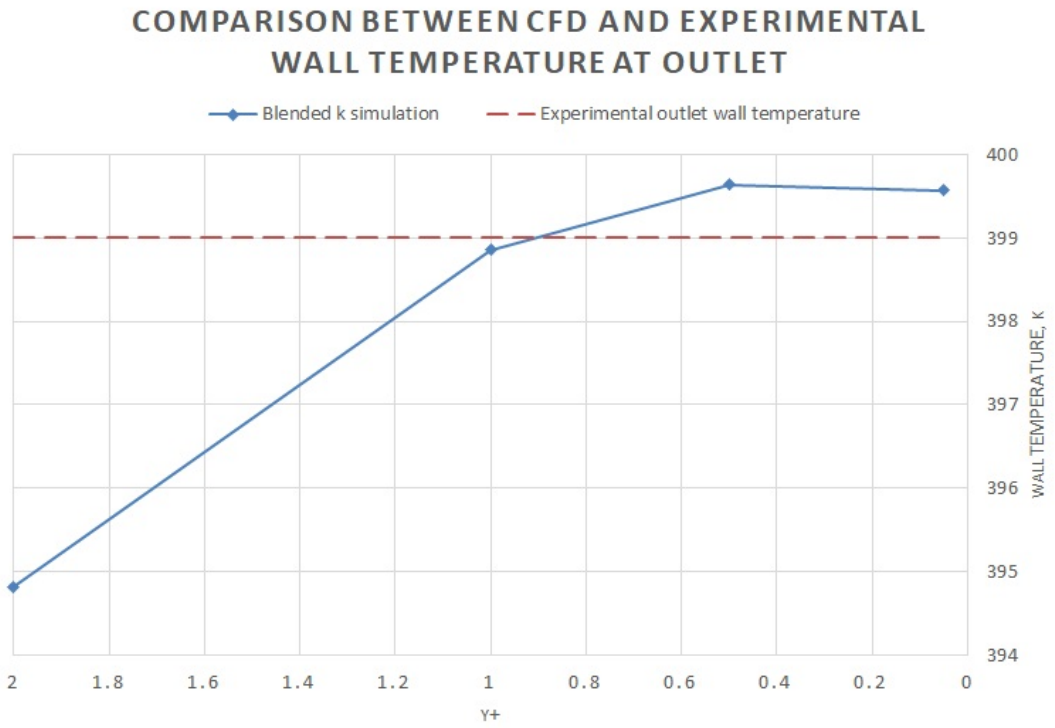

Figure 5.29: Wall temperature at outlet- Blended k simulation

5.2.2.4.7.1 Results After the mesh study's finding that the model is good for meshes with y^+ less than 1, a mesh with $y^+ = 0.5$ was used to obtain the results for the different heat flux cases from the experiment. Figure 5.30 shows the heat transfer coefficient comparison between CFD, experiment, and the correlations. It is clearly seen that the blended thermal conductivity function gives better results compared to both linearly varying and constant thermal conductivity. An important point is that the tuning coefficient used to modify the thermal conductivity is tuned for each heat flux case. The tuning coefficients used for each heat flux are tabulated in Table 5.10.

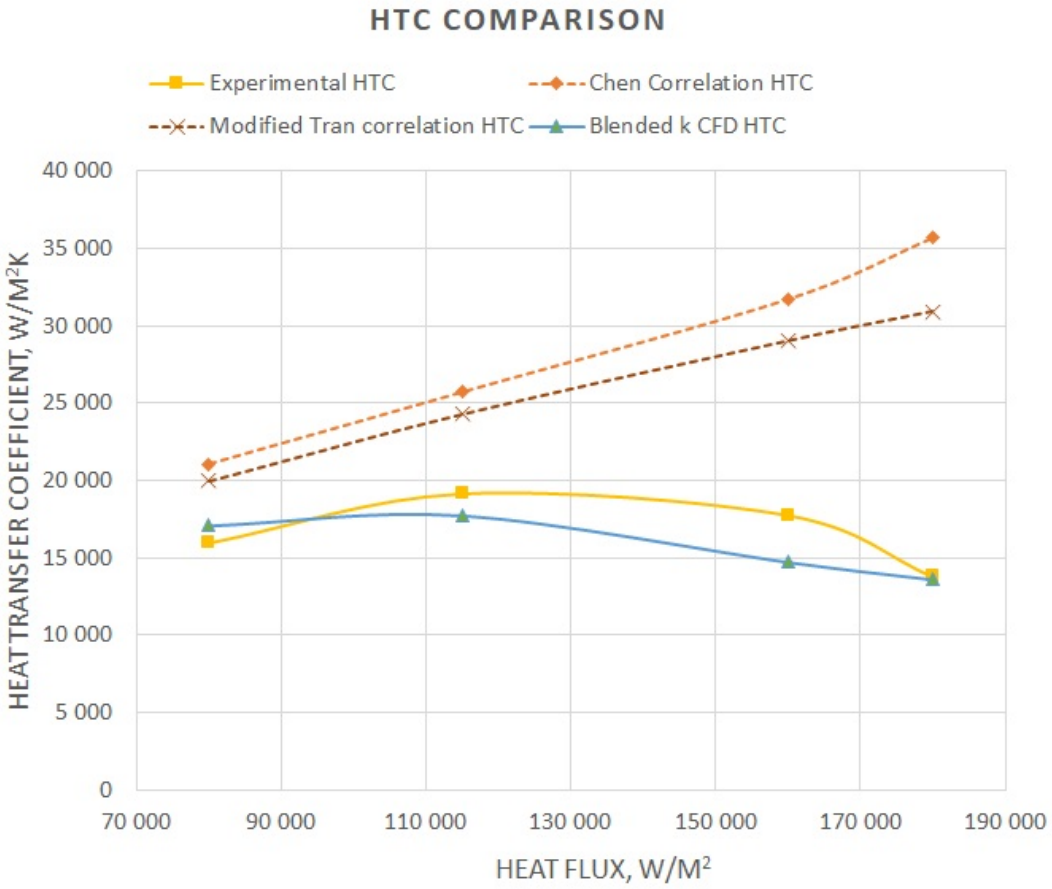

Figure 5.30: HTC comparison - Blended k simulation

Table 5.10: Heat Flux and Tuning Coefficient Data

Heat Flux (W/m^2)	**Tuning Coefficient (C_k)**
80,000	5
115,000	12
160,000	55
180,000	140

5.2.2.4.8 Comparison between Bulk Quantities Even though the wall temperature was comparatively very different between the varying and constant thermal conductivity simulations, the bulk parameters were not significantly different between the simulations. The bulk temperature of the fluid at the outlet of the test section was obtained by mass averaging the static temperature at the outlet. The results are tabulated in Table 5.11. From the table, it can be seen that the maximum difference between the different simulations was less than 0.2%.
Figure 5.31 shows the outlet vapor quality, which is compared with the varying and constant thermal conductivity simulations along with the theoretically calculated

Table 5.11: Comparison of bulk temperature

Heat Flux (W/m^2)	Constant k Bulk Temperature (K)	Varying k Bulk Temperature (K)	Blended k Bulk Temperature (K)
80,000	391.57	391.50	391.57
115,000	393.44	393.88	393.47
160,000	395.80	395.12	395.90
180,000	396.92	396.80	396.90

vapor quality, which was calculated from the heat balance equation. It can be seen that there is complete agreement between the vapor qualities of the three simulation cases and the theoretical vapor quality.

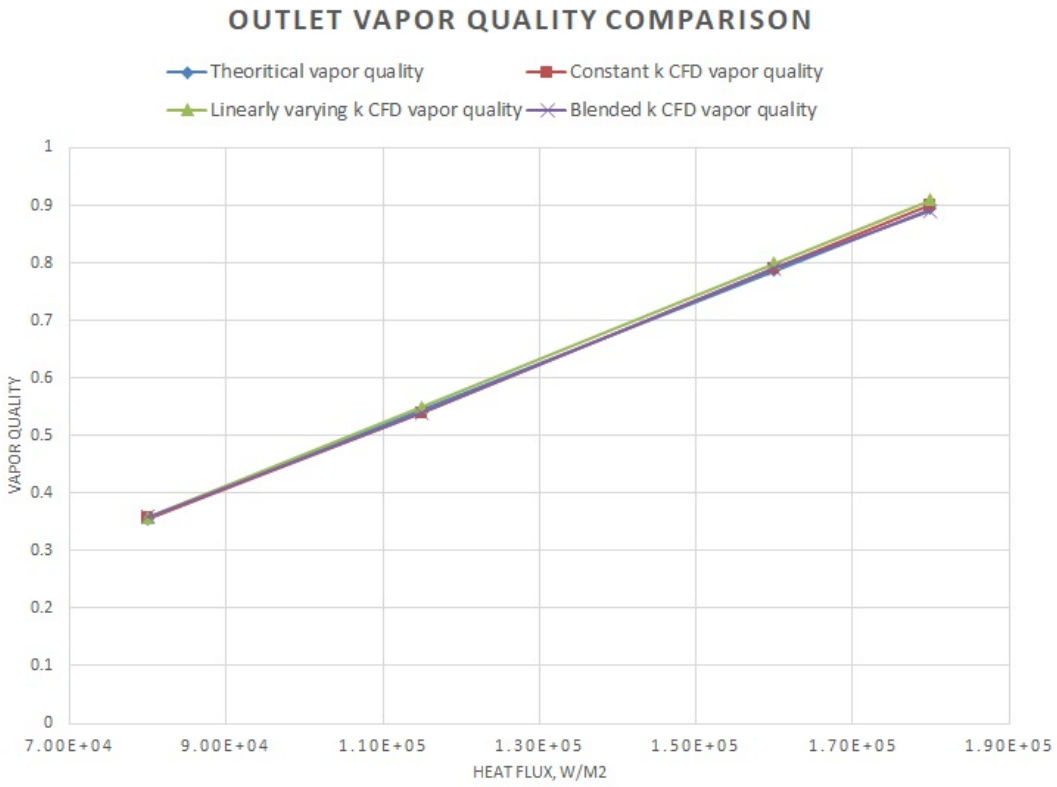

Figure 5.31: Outlet vapor quality

From these analyses, it is clear that the thermal conductivity affecting the wall temperatures has no impact on bulk quantities like bulk temperature and vapor quality at the exit.

5.2.2.4.9 Pressure Drop The pressure drop along the pipe can be significantly impacted by the interaction between the liquid and vapor phases. Figure 5.32 shows the pressure drop plotted for different heat flux cases that were simulated using linearly varying, constant, and blended thermal conductivity UDFs, along with the two-phase pressure drop correlation given by Lockhart and Martinelli. However,

the pressure drop shows about 99% deviation between the CFD simulations for all three cases and the pressure drop correlation. The CFD simulations' pressure drop is similar to the single-phase pressure drop, where only liquid water flows through the pipe, compared to the Darcy Weisbach equation using the Blasius correlation to find the friction factor.

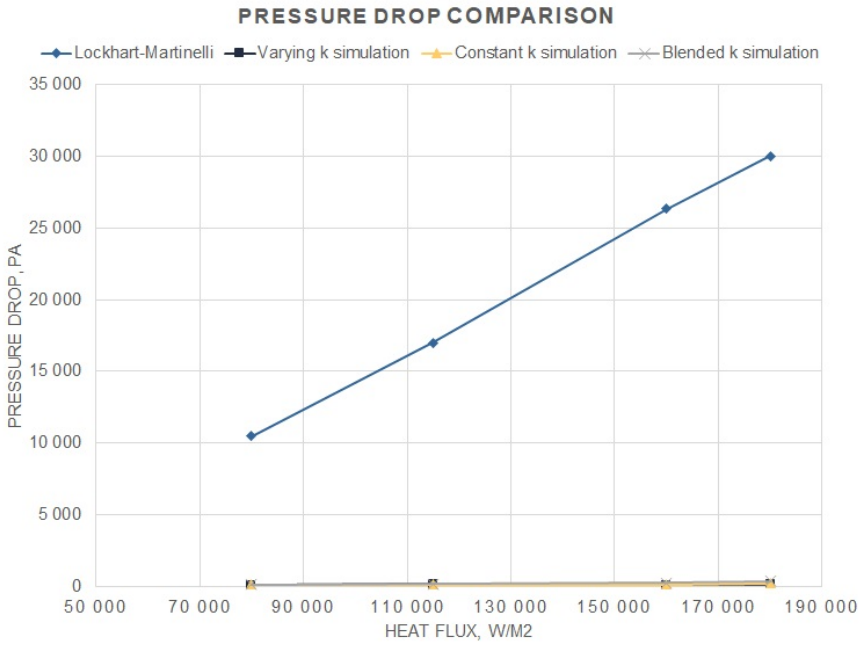

Figure 5.32: Two-phase pressure drop comparison

6
Conclusion

The tuned single phase simulations of the boiling behavior in horizontal pipes of a heat exchanger has revealed several key findings. Firstly, it is observed that the tuned material model shows some great strength in predicting the bulk quantities quite consistent between the different thermal conductivity models.

However the prediction of near wall parameters like the wall temperature has been quite inconsistent with the near wall refinement with mesh. The primary reason for this discrepancy is attributed to the effective thermal conductivity change near the walls with respect to finer meshes. It was found that the lesser influence of the turbulent quantities near the wall for finer mesh is causing the effective thermal conductivity to drop massively for finer meshes thereby having its impact on the wall temperature.

Further analysis of the influence of thermal conductivity, the mesh study with having a constant thermal conductivity that of liquid water instead of a linearly varying thermal conductivity showed consistent wall temperatures and when compared to the experimental heat transfer coefficient, it showed great comparability with the results having a maximum deviation of 25% which is lesser than that of heat transfer correlations as they have an average deviation of 30%.

After understanding the influence of thermal conductivity near the walls, it was understood that the lack of mixing between the phases near the walls was the main reason for the wall temperature rise. In order to counteract this lack of mixing, a blended function was to vary thermal conductivity for inducing the mixing more. The blended function's coefficient was tuned for different cases as like some of the multiphase models to properly match the experimental results and the heat transfer coefficients between the experiments and blended thermal conductivity showed greater agreement than the other two cases.

7
Recommendations for future work

1. Validation of the tuned model against diverse experiments and working fluids under various operating conditions would significantly enhance the understanding of the model's accuracy.
2. Further analysis of the thermal conductivity effect on wall properties, such as wall temperature for finer meshes, and understanding its influence will greatly help to further develop the model. Another interesting parameter to alter and observe its effects on the results is the wall Prandtl number or turbulent Prandtl number in ANSYS Fluent, as this might provide insights since the wall temperature shows significant deviation.
3. Another important parameter that needs re-evaluation is the pressure drop, which was very similar to the single-phase pressure drop. The reasons for the absence of a pressure drop due to boiling need to be investigated, as the reasons for this behavior are currently unknown.
4. The blended thermal conductivity UDF can be improved by determining the tuning coefficient based on a parameter such as the theoretical vapor quality, instead of performing repeated simulations to find the tuning coefficient for each flow case.

Bibliography

[1] *2.* URL: https://aeroreport.de/en/good-to-know/a-brief-guide-how-the-wet-concept-works.

[2] *1.* URL: https://www.mtu.de/newsroom/press/press-archive/press-archive-detail/clean-aviation-switch-project-to-advance-hybrid-electric-and-water-enhanced-turbofan-technologies/.

[3] Yunus A. Cengel and John M. Cimbala. *Fluid Mechanics - Fundamentals and Applications*. 2014.

[4] Yunus A. Cengel and Afshin J. Ghajar. *Heat and Mass Transfer*. 2015.

[5] M. Ilić, M. M. Petrović, and V. Stevanović. "Boiling heat transfer modelling: a review and future prospectus". In: *International Journal of Thermal Sciences* 23.1 (2019), pp. 87–107.

[6] Sarit Kumar Das and Dhiman Chatterjee. *Vapor Liquid Two Phase Flow and Phase Change*. 2023.

[7] K. Stephan. *Heat Transfer in Condensation and Boiling*. Vol. 1. Berlin: Springer-Verlag, 1992, p. 84.

[8] L. Wojtan, T. Ursenbacher, and J. R. Thome. "Investigation of flow boiling in horizontal tubes: Part II—Development of a new heat transfer model for stratified-wavy, dryout and mist flow regimes". In: *International Journal of Heat and Mass Transfer* 48.14 (2005), pp. 2970–2985.

[9] J. Dirker et al. "Thermal Energy Processes in Direct Steam Generation Solar Systems: Boiling, Condensation and Energy Storage–A Review". In: *Frontiers in Energy Research* 6 (2019), p. 147.

[10] J. M. Mandhane, G. A. Gregory, and K. Aziz. "A flow pattern map for gas—liquid flow in horizontal pipes". In: *International Journal of Multiphase Flow* 1.4 (1974), pp. 537–553.

[11] L. Cheng, G. Ribatski, and J. R. Thome. "Two-phase flow patterns and flow-pattern maps: fundamentals and applications". In: *International Journal of Heat and Fluid Flow* 32.2 (2008), pp. 246–253.

[12] Lewis F. Moody. "Friction factors for pipe flow". In: *Transactions of the American Society of Mechanical Engineers* 66.8 (1944), pp. 671–678.

[13] B. S. Massey. *Mechanics of Fluids*. 8th. Equation 7.5. Taylor & Francis, 2006, p. 254. ISBN: 978-0-415-36205-4.

[14] E. R. G. Eckert. "Engineering relations for heat transfer and friction in high-velocity laminar and turbulent boundary-layer flow over surfaces with constant pressure and temperature". In: *Chemical Engineering Science* 78.6 (1956), pp. 1273–1283.

[15] F. W. Dittus and L. M. K. Boelter. “Heat transfer in automobile radiators of the tubular type”. In: *University of California Publications in Engineering* 12.1 (1985), pp. 3–22.

[16] E. N. Sieder and G. E. Tate. “Heat transfer and pressure drop of liquids in tubes”. In: *Industrial & Engineering Chemistry* 28.12 (1936), pp. 1429–1435.

[17] V. Gnielinski. “New equations for heat and mass-transfer in turbulent pipe and channel flow”. In: *International Journal of Heat and Mass Transfer* 16.2 (1976), pp. 359–368.

[18] R. C. Martinelli and R. W. Lockhart. “Proposed correlation of data for isothermal two-phase, two-component flow in pipes”. In: *Chemical Engineering Progress* 45.1 (1949), pp. 39–48.

[19] D. Chisholm. “A theoretical basis for the Lockhart-Martinelli correlation for two-phase flow”. In: *International Journal of Heat and Mass Transfer* 10.12 (1967), pp. 1767–1778.

[20] J. C. Chen. “Correlation for boiling heat transfer to saturated fluids in convective flow”. In: *Industrial & Engineering Chemistry Process Design and Development* 5.3 (1966), pp. 322–329.

[21] W. Yu et al. “Two-phase pressure drop, boiling heat transfer, and critical heat flux to water in a small-diameter horizontal tube”. In: *International Journal of Multiphase Flow* 28.6 (2002), pp. 927–941.

[22] T. N. Tran, M. W. Wambsganss, and D. M. France. “Small circular- and rectangular-channel boiling with two refrigerants”. In: *International Journal of Multiphase Flow* 22 (1996), pp. 485–498.

[23] Z. Liu and R. H. S. Winterton. “A general correlation for saturated and subcooled flow boiling in tubes and annuli, based on a nucleate pool boiling equation”. In: *International Journal of Heat and Mass Transfer* 34.11 (1991), pp. 2759–2766.

[24] D. C. Groeneveld, S. C. Cheng, and T. Doan. “1986 AECL-UO critical heat flux lookup table”. In: *Heat Transfer Engineering* 7.1-2 (1986), pp. 46–62.

[25] B. K. Hardik and S. V. Prabhu. “Boiling pressure drop and local heat transfer distribution of water in horizontal straight tubes at low pressure”. In: *International Journal of Thermal Sciences* 110 (2016), pp. 65–82.

[26] N. Kattan, J. R. Thome, and D. Favrat. “Flow boiling in horizontal tubes. Part 3: Development of a new heat transfer model based on flow patterns”. In: *International Journal of Heat and Mass Transfer* 120.1 (1998), pp. 156–165.

[27] H. Deng, M. Fernandino, and C. A. Dorao. “Flow boiling in a horizontal tube at high vapor qualities”. In: *American Society of Mechanical Engineers* 50343 (2016).

[28] D. Jige, K. Sagawa, and N. Inoue. “Effect of tube diameter on boiling heat transfer and flow characteristic of refrigerant R32 in horizontal small-diameter tubes”. In: *International Journal of Refrigeration* 76 (2017), pp. 206–218.

[29] Inc. ANSYS. *Ansys Fluent Theory Guide*. 2023.

[30] Brian Launder and DB Spalding. “Turbulence modelling”. In: *Com. Mech. Appl. Mech. Eng* 3 (1974), p. 269.

[31] F. R. Menter. “Performance of Popular Turbulence models for attached and separated adverse pressure gradient flows”. In: *AIAA Journal* 30 (1992), p. 2066.

[32] H. R. Hiester et al. “Assessment of Spurious Mixing in Adaptive Mesh Simulations of the Two-Dimensional Lock-Exchange”. In: *Ocean Modelling* 73 (2014), pp. 30–44.

8

Appendix

8.1 Appendix A - Density UDF

```
#include "udf.h"

DEFINE_EXECUTE_AT_END(density_change)
{
Domain *d;
Thread *t;
real xc[ND_ND];
cell_t c;
real h;
real h_l = 398602.5;
real h_g = 2600102.5;
real h_lg = 2201500;
real vapor_quality;
real rho_l = 943;
real rho_g = 1.13;
d = Get_Domain(1); thread_loop_c(t,d)
{
begin_c_loop(c,t)
h=C_H(c,t); if ( h <= h_l)
{
C_R(c,t) = rho_l;
}
else if (h > h_l && h <= h_g)
{
vapor_quality = (h- h_l) / h_lg; C_UDMI(c,t,0) = vapor_quality;
C_R(c,t) = vapor_quality * rho_g + (1- vapor_quality)*rho_l;
}
else
{
C_R(c,t) = rho_g;
}
end_c_loop(c,t)

}
```

8.2 Appendix B - Specific heat UDF

```
DEFINE_SPECIFIC_HEAT(cp_new, T, Tref, h, yi)
{
cell_t c;
Thread *t;
real cp;
real delT = 10;
real b_start = 388;
real b_end = 398;
real b_middle = (b_start + b_end)/2;
real h_l = 398602.5;
real h_g = 2600102.5;
real h_lg = 2201500;

real cp_l = 4244; real cp_g = 2178;

real div_factor; real cp_max;

real enthalpy_bp;
enthalpy_bp = h_l + h_lg*((b_middle-b_start)/delT); cp_max = (2*h_lg)/delT;
div_factor = enthalpy_bp / cp_max ;


if(T >= b_start && T <= b_middle)
{
*h = h_l + h_lg*((T-b_start)/delT); return *h/div_factor;
}

if(T > b_middle && T <= b_end)
{
*h = h_l +h_lg*((T-b_start)/10); return cp_g + (h_g - *h)/div_factor;
}


if(T > b_end)
{
*h = h_l+h_lg+cp_g*(T-398); return cp_g;
}

}
```

8.3 Appendix C - Viscosity UDF

```
#include "udf.h"

DEFINE_PROPERTY(viscosity,c,t)
{
real mu;
real mu_g = 0.0000129;
real mu_l= 0.0002325;
real h;
real h_l = 398602.5;
real vapor_quality;
real h_g = 2600102.5;
real h_lg = 2201500;

h = C_H(c,t); if (h <= h_l)
{
mu = mu_l;
}
else if (h> h_l && h <= h_g)
{
vapor_quality = (h- h_l) / h_lg;
mu = vapor_quality * mu_g + (1-vapor_quality)*mu_l;

}

else if (h > h_g)
{
mu = mu_g;
}

return mu;

}
```

8.4 Appendix D - Varying thermal conductivity UDF

```
#include "udf.h"

DEFINE_PROPERTY(thermal_conductivity,c,t)
{
real k;
real k_g = 0.0256;
real k_l= 0.6;
real h;
real h_l = 398602.5;
real vapor_quality;
real h_g = 2600102.5;
real h_lg = 2201500;


h = C_H(c,t); if (h <= h_l)
{
k = k_l;
}
else if (h> h_l && h <= h_g)
{
vapor_quality = (h- h_l) / h_lg;
k = vapor_quality * k_g + (1-vapor_quality)*k_l;

}

else if (h > h_g)
{
k = k_g;
}

return k;
}
```

8.5 Appendix E - Blended thermal conductivity UDF

```
#include "udf.h"

DEFINE_PROPERTY(thermal_conductivity,c,t)
{
real k;
real k_g = 0.0256;
real k_l= 0.6;
real h;
real h_l = 398602.5;
real vapor_quality; real h_g = 2600102.5;
real h_lg = 2201500;
real constant;

constant = (k_l) /(2*k_g) ; h = C_H(c,t);
if (h <= h_l)
{
k = k_l;
}
else if (h> h_l && h <= h_g)
{
vapor_quality = (h- h_l) / h_lg;
k = constant*(vapor_quality * k_g + (1-vapor_quality)*k_l);

}

else if (h > h_g)
{
k = (constant)*k_g;
}
return k;
}
```

DEPARTMENT OF SOME SUBJECT OR TECHNOLOGY
CHALMERS UNIVERSITY OF TECHNOLOGY
Gothenburg, Sweden
www.chalmers.se

CHALMERS
UNIVERSITY OF TECHNOLOGY